JOC The Journal of Organic Chemistry

pubs.acs.org/joc Article

Synthesis and Photoswitching Properties of Bioinspired Dissymmetric γ-Pyrone, an Analogue of Cyclocurcumin

Jérémy Pecourneau, Raúl Losantos, Antonio Monari, Stéphane Parant, Andreea Pasc,* and Maxime Mourer*

Cite This: J. Org. Chem. 2021, 86, 8112–8126 Read Online

ACCESS | Metrics & More | Article Recommendations | Supporting Information

ABSTRACT: Cyclocurcumin (CC), a turmeric curcuminoid with potential therapeutic properties, is also a natural photoswitch that may undergo *E*/*Z* photoisomerization under UV light. To be further exploited in relevant biological applications, photoactivation under near-infrared (NIR) irradiation is required. Such requirement can be met through opportune chemical modifications, by favoring two-photon absorption (TPA) probability. Herein, a general and efficient synthesis of a biomimetic 2,6-disubstituted-γ-pyrone analogue of CC is described, motivated by the fact that molecular modeling previews an order of magnitude increase of its NIR TPA compared to CC. Three retrosynthetic pathways have been identified (i) *via* an aryl-oxazole intermediate or *via* aryl-diynone through (ii) a bottom-up or (iii) a top-down approach. While avoiding the passage through unstable synthons or low-yield intermediate reactions, only the latest approach could conveniently afford the 2,6-disubstituted-γ-pyrone analogue of CC, in ten steps and with an overall yield of 18%. The photophysical properties of our biomimetic analogue have also been characterized showing an improved photoisomerization yield over the parent natural compound. The potentially improved nonlinear optical properties, as well as enhanced stability, may be correlated to the enforcement of the planarity of the pyrone moiety leading to a quadrupolar D−π−A−π−D system.

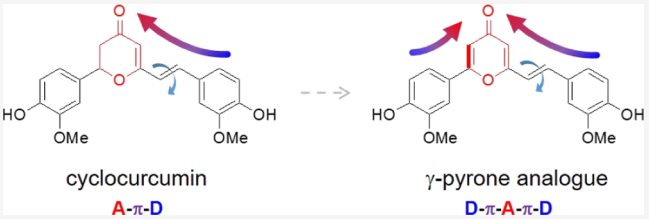

1. INTRODUCTION

Molecular photoswitches are compounds capable to reversibly populate, under the effect of an external perturbation such as the absorption of electromagnetic light, two different stable states, that is, conformation or configuration of isomers that should ideally exhibit significantly different geometries and photochromic properties. The capability of controlling the interconversion between the two states is clearly extremely beneficial in potentially providing molecular-based smart materials or devices, as well as molecular machines converting light energy into mechanical work.

Although their potential is still far from being fully explored, both synthetic and natural photoswitches already have a wide range of applications, including optogenetics and imaging, biotechnology, or pharmacology.

The most well-known natural photoswitch is the chromophore of the transmembrane rhodopsin protein, that is, the protonated Schiff-base of 11-*cis* retinal, which following the absorption of visible light switches into all-*trans*-retinal to initiate the cascade leading either to transmembrane ion transport in bacteria or to vision in superior animals. Most notably, rhodopsin-embedded retinal is also one of the most extremely efficient switches both considering the high quantum yield (approaching 80%) and the ultrafast reaction (around 120 fs). The molecular and photochemical bases, in terms of the topology of the involved potential energy surfaces (PESs) at the base of such efficiency, have been deeply characterized by both time-resolved spectroscopy and computational photochemistry,[1] while recently possible dark-photochemistry-based isomerization related to photodynamic therapy side effects have also been unraveled.[2] The combined use of the biomimetic strategy and the opportune molecular design is clearly beneficial in improving photoswitching capabilities.[3] Several other molecular photoswitches have been reported to date, that is, 9-aryl-phenalenones whose photocyclization is the key step in the defense mechanism of plants against pathogens[4] or flavylium derivatives, bioinspired from anthocyanins, the natural colorants of most red and blue flowers and fruits.[5]

Herein, we report the first bioinspired photoswitch derived from cyclocurcumin (CC). As a matter of fact, CC is a natural compound (Scheme 1) that can be isolated in small amounts from turmeric rhizomes (*Curcuma longa*). Despite the fact that the remarkable potential pharmacological properties of curcumin are by far driving the most interest, more recent studies revealed the antioxidant, antivasoconstrictive, immune-

Received: March 12, 2021
Published: June 8, 2021

https://doi.org/10.1021/acs.joc.1c00598
J. Org. Chem. 2021, 86, 8112–8126

Scheme 1. Natural CC and Its 2,6-Disubstituted-γ-pyrone Analogue

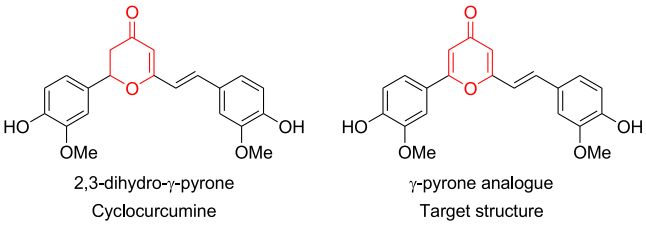

modulating, and neuroprotective effects of CC. However, photoswitching properties of CC were only scarcely investigated, even though they have been demonstrated and rationalized computationally, together with their dependence on environmental factors.[6]

CC has an α,β-unsaturated dihydropyrone moiety that allows the *trans*−*cis* photoisomerization of the β ethylenic bond (Scheme 1).[7] The predominant form of CC both in natural compounds and in solution is the *trans* isomer, which is thermodynamically most favorable. Direct *trans*−*cis* isomerization of CC occurs under irradiation at around λ_{max} = 375 nm, while the reverse reaction takes place thermally or photochemically following the exposure to 300 nm light. CC also exhibits fluorescence emission at around 500 nm, as a function of the solvent. Interestingly, molecular modeling suggests that the competition between the two excited-state relaxation routes, photoisomerization versus fluorescence, is strongly dependent on the polarity of the environment, which ultimately determines the observed outcome.[6] The competition between the two processes, especially in complex and inhomogeneous biological environments, is detrimental to achieve an exploitable quantum yield. Indeed, an ideal molecular photoswitch should be chemically stable, should have a high photoisomerization yield, large spectral differences between the isomers, and low fatigue, that is, the ability of optical resetting.

Furthermore, in order to be exploitable in biomedical applications and especially in photopharmacology, a chromophore should exhibit significant absorption in the biological optical active window, that is cover the 650 to 1350 nm range in the NIR region. As previously said, photoswitching of CC is instead induced by absorption in the UVA region, and hence, results inapplicable in a biological environment due to the limited penetration and the possible toxicity of the incident light. One way to circumvent such a limitation resides in exploiting nonlinear and, in particular, two-photon absorption (TPA) properties. Indeed, in this case, the simultaneous absorption of two photons having a wavelength of about 740 nm would be sufficient to populate the isomerizing excited state. Furthermore, TPA probability has a quadratic dependence on the light-source intensity; hence, it decays more rapidly when moving away from the incident laser focal point, allowing for better control of the spatial selectivity that is extremely important in biomedical applications, such as photodynamic therapy. While we have shown that natural CC has a relatively high TPA cross section compared to analogous organic compounds, the calculated value of 14 GM is still too low for its veritable exploitation.[6] For all these reasons, we designed herein an analogue of CC with improved nonlinear absorption properties and especially with a significantly increased TPA cross section.

We thus propose a 2,6-disubstituted-γ-pyrone analogue (Scheme 1) with an additional ethylene bond compared to the 2,3-dihydro-γ-pyrone core of CC to (i) increase the planarity of the structure and to (ii) introduce a second donor−acceptor group (aryl-ketone) increasing the molecular symmetry. Indeed, planar and quadrupolar structures D−π−A−π−D, such as the one of pyrone, are expected to be more efficient in TPA than their dipolar analogues D−π−A, such as CC.[8]

2. RESULTS AND DISCUSSION

2.1. Equilibrium Geometry. TPA cross-section efficiency in organic compounds can be easily related to their molecular structures. TPA efficiency is founded on a rather complex theory, developed by Maria Göppert-Mayer in 1931, and based on the presence of intermediate fictive states allowing to overcome the formally quantum-physically prohibited simultaneous absorption of two photons. However, practical rules of the thumb relating to TPA efficiency and the specific molecular architecture exist and can be used. In particular, it can be shown that planar and centrosymmetric arrangements are extremely beneficial to increase the TPA cross section. Analogously, the presence of charge-transfer excited states can also be pointed out for its most favorable influence. More

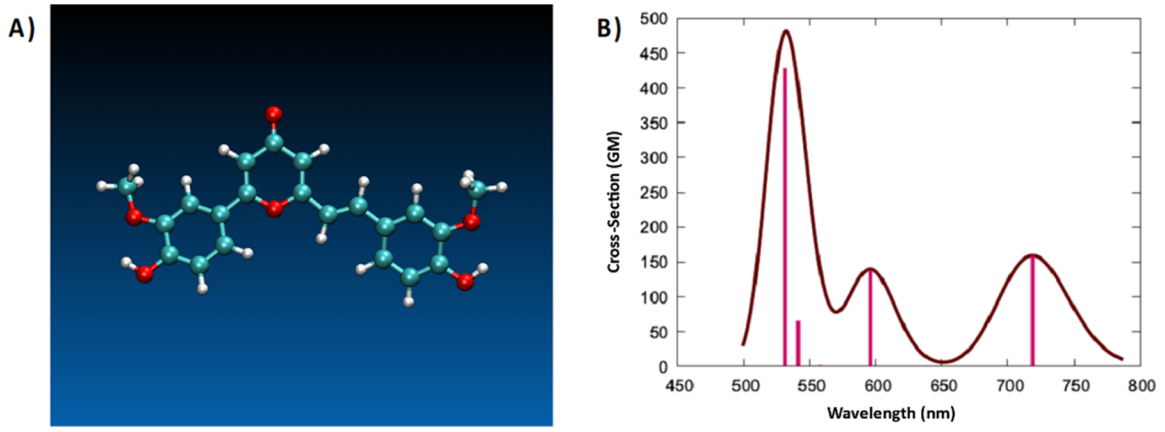

Figure 1. Equilibrium ground-state geometry simulated at the DFT level (A) and TPA absorption spectrum (B) of our targeted 2,6-disubstituted-γ-pyrone **1** calculated at CAM-B3LYP level of theory. Note that the absorption spectrum has been obtained by convoluting the vertical transitions, represented as vertical sticks, with Gaussian functions of fixed-width at a half-length of 0.3 eV.

https://doi.org/10.1021/acs.joc.1c00598
J. Org. Chem. 2021, 86, 8112−8126

Scheme 2. Retrosynthetic Pathways for the Formation of Dissymmetric γ-Pyrone 1

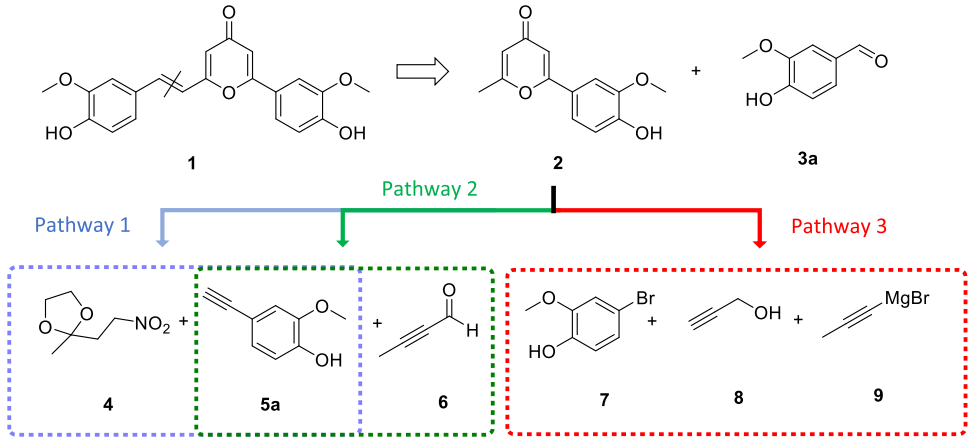

specifically, quadrupolar molecules exhibiting an alternation of donor (D) and acceptor (A) units linked by conjugated bridges (π), that is, D−π−A−π−D structures, are the most favorable molecular scaffolds to achieve high and exploitable cross sections and are more efficient than their dipolar analogues D−π−A, such as CC.[8] When examining the molecular formula and the equilibrium geometry of CC, the breaking of the planarity induced by the free rotation of the phenyl group in position two can be seen as a further reason for the simulated moderate cross section for the naturally occurring compound. To fix the planarity issue, the most promising possibility could be to introduce a double bond leading to a pyrone core. Indeed, the optimization of the geometry of thermodynamically favored *E*-isomer of γ-pyrone, performed by DFT, has shown the quasiplanarity of the organic core (Figure 1) as also quantified by the dihedral angle between the phenyl ring and the pyrone moiety that reaches the value of 160° in contrast to the almost perpendicular arrangement observed for natural CC.

The influence of oxidation on the linear optical properties of our targeted compound, as obtained by state-of-the-art molecular modeling, will be discussed in the following section. Here, to justify the forthcoming synthetic efforts, we only report the simulated TPA spectrum in water that would be the most relevant solvent for biological applications. Note that, as detailed in Section 2.3.1, the CAM-B3LYP functional is the one that better reproduces the optical properties of our compound, and hence, was retained for modeling TPA. Figure 1 shows simulated TPA previews that the nonlinear absorption to the S_1 (π−π^*) state will take place in the NIR region, with a maximum at 719 nm. Notably, the corresponding band is well separated from the one leading to the S_2 (n−π^*) absorption, and most importantly, it is characterized by a cross section of 159 GM. This value represents an order of magnitude increase in the TPA performance over the parent CC, which peaked at only 14 GM in the NIR range.[6] This could be also assigned to the enhancement of planarity of the scaffold that leads to a quadrupolar arrangement of the D−π−A−π−D type. Remarkably, absorption to the S_2 state also led to a band whose tails would partially cover the biological active window, peaking at around 600 nm and having a cross section of 139 GM. Absorption to higher excited states leads to the band appearing in the visible part of the spectrum, and hence, being less exploitable despite its high cross section.

Globally, the results of molecular modeling are consistent in previewing a considerable increase of the optical properties of the target biomimetic analogue, thus justifying the efforts in synthetic methodology that have been undertaken and that are presented in the following section.

2.2. Synthesis of the 2,6-Disubstituted-γ-Pyrone Analogue of CC. The retrosynthetic pathway proposed herein for the synthesis of the targeted 2,6-disubstituted-γ-pyrone analogue of CC is given in Scheme 2. This consists of the aldolization/crotonization reaction of alkylated vanillin and the methyl group of γ-pyrone **1** and leading to a photoisomerizable carbon−carbon double bond.

Our strategy was based on the formation of the γ-pyrone ring, the di-dehydrogenated equivalent of the 2,4-dihydro-γ-pyrone ring, present in CC. Various synthetic routes affording to symmetrically or asymmetrically in 2,6 positions were already described in the literature according to classical methods such as (i) the cyclocondensation of dienol of 1,3,5-tricarbonyl compounds under mild acidic catalysis (*i.e.*, Brønsted acids such as triflic acid or *p*-toluenesulfonic acid) and[9,10] (ii) the cyclization of diynone,[11−13] or *via* an original pathway using an isoxazole intermediate.[14] Herein, we chose to implement the strategies involving either a diynone intermediate, as the most explored and documented pathway to form a γ-pyrone ring, or an oxazole intermediate a priori faster and offering good yields. Thus, three synthetic ways were evaluated for the formation of the central pyrone moiety, namely, (i) with nitro and terminal alkyne fragments **4** and **5a** (pathway 1, Scheme 2), (ii) alkyne **5a** and butynal **6** (pathway 2, Scheme 2), or (iii) bromoguaiacol **7**, propargyl alcohol **8**, and 1-propynylmagnesium bromide **9** (pathway 3, Scheme 2).

In the first pathway, the synthesis of **2** was envisaged through the synthesis of isoxazole intermediate **11**, which is previously generated from the two building blocks **4** and **5a** (Scheme 2, Pathway 1). This procedure is similar to the one previously reported in studies by Li and Lacasse, and it is based on the 1,3-dipolar cycloaddition reaction between acetylene **5a** and nitrile oxide, generated *in situ* from fragment **4**.[14] According to the authors, the presence of the 2-oxoalkyl chain in position three of isoxazole should allow after reduction by $Mo(CO)_6$ an enamino ketone intermediate, which is cyclized under acidic conditions into corresponding γ-pyrone **2**.

The general reaction scheme corresponding to the first retrosynthetic pathway is given in Schemes 3 and 4.

https://doi.org/10.1021/acs.joc.1c00598
J. Org. Chem. 2021, 86, 8112−8126

Scheme 3. Synthetic Pathway to Obtain Terminal Alkyne 5

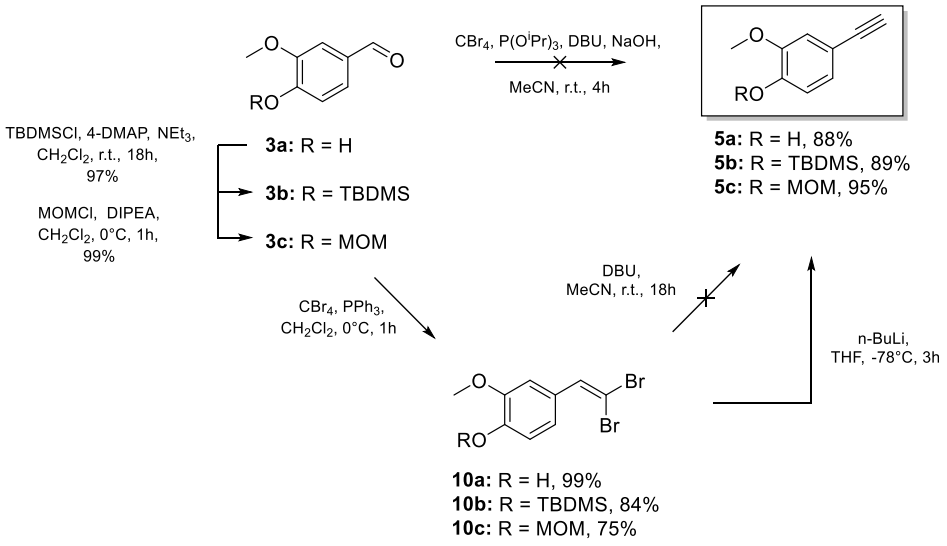

Scheme 4. First Strategy Considered to Obtain 2-Aryl-γ-pyrone 2

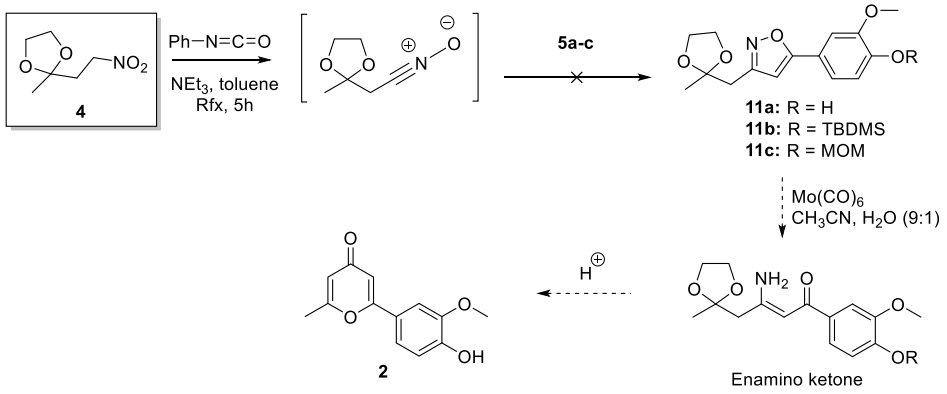

Scheme 5. Bottom-Up Approach to Obtain 2-Aryl-γ-pyrone 2

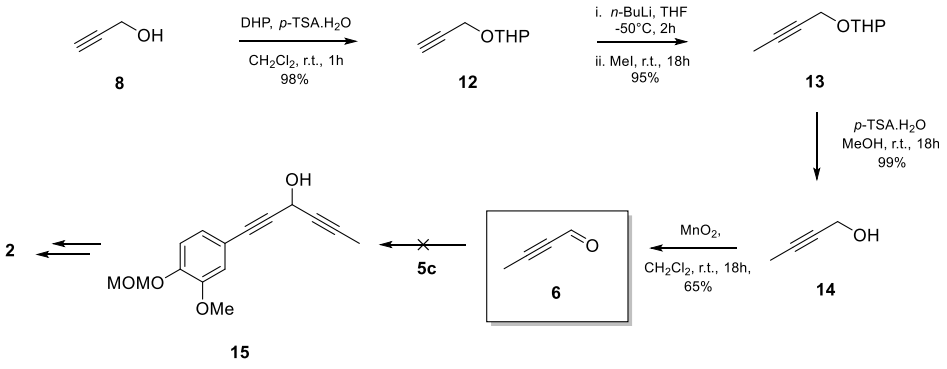

Compounds **5a−c** (Scheme 3) could have been obtained one pot by transforming the aldehyde group of vanillin derivatives (**3a−c**) into terminal alkyne as proposed in studies by Doddi et al.[15] This implies the use of modified Ramirez olefination[16,17] [CBr_4 and triisopropyl phosphite $P(O^iPr)_3$ to avoid the elimination of triphenylphosphine oxides], followed by modified Corey−Fuchs reaction using 1,8-diazabicyclo[5.4.0]-undec-7-ene (DBU) and NaOH as bases. Unfortunately, terminal alkynes **5a−c** could not be obtained according to this method. Thus, the synthesis was done in two steps involving (i) the Ramirez olefination of aldehyde to give 1,1′-dibromoalkenes **10a−c** in good yields and (ii) Corey−Fuchs reaction (Scheme 3).[18,19] For this latest way, the reaction performed with DBU only led to very low yields (<10%).[20] Finally, the classical Corey−Fuchs reaction carried out with *n*-BuLi as the base at −78 °C gave the desired terminal alkynes **5a−c** with an excellent yield (Scheme 3).

In parallel, synthon **4** was prepared, according to the literature, from methyl vinyl ketone and sodium nitrite in acidic conditions, followed by carbonyl protection as dioxolane.[21,22] However, in our experiments, the two reaction steps afforded yields lower than 30% as well as to the formation

https://doi.org/10.1021/acs.joc.1c00598
J. Org. Chem. 2021, 86, 8112−8126

Scheme 6. Top-Down Approach Leading to γ-Pyrone Core 2

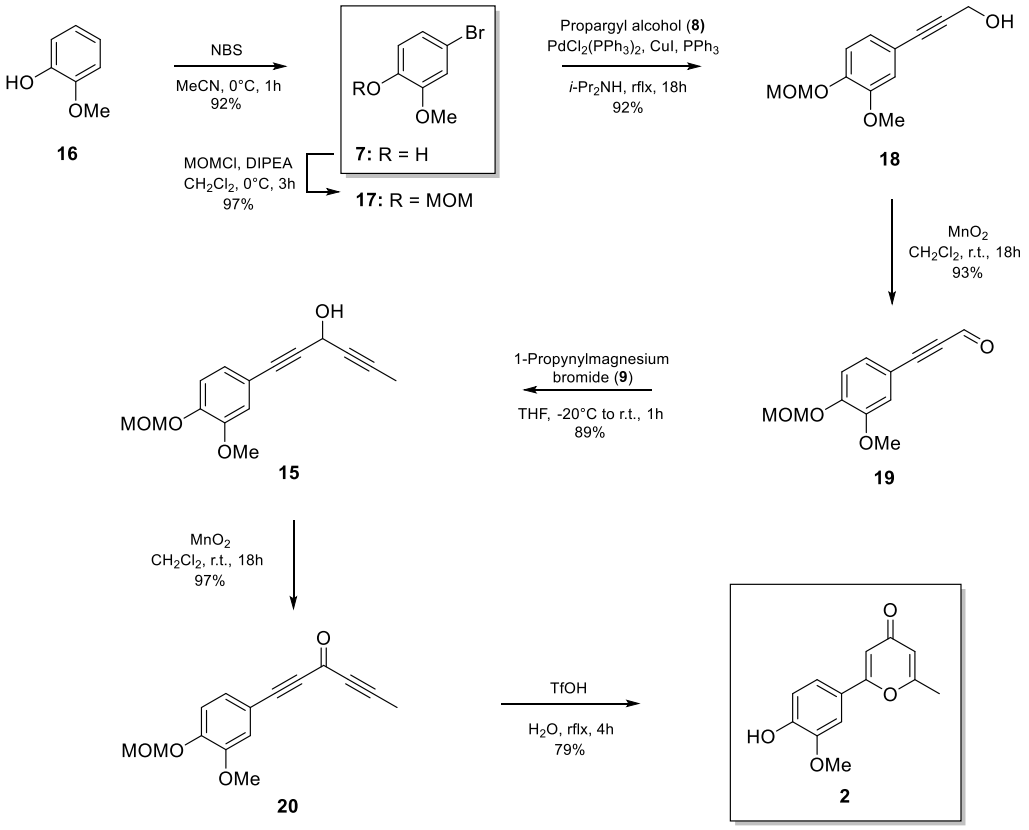

Scheme 7. Synthetic Pathway Leading to the 1, 2,6-Disubstituted-γ-pyrone Analogue of CC

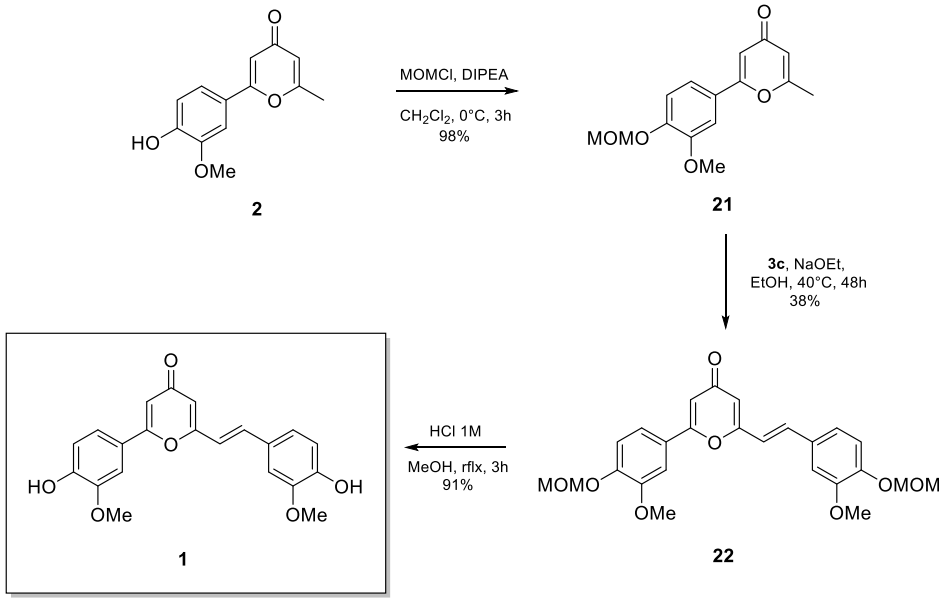

of 1,4-adduct of acetate on conjugated carbonyl as the main product. Then, the conversion of **4** into the corresponding nitrile oxide precursor was tested *in situ* under Mukaiyama's dehydration conditions using phenyl isocyanate.[23] Unfortunately, the expected heterocyclic compounds **11a–c** could not be isolated, probably due to the instability of nitro derivative **4** or the nonformation *in situ* of the nitrile oxide intermediate (Scheme 4). Therefore, this strategy was not further explored.

The second pathway envisaged that the formation γ-pyrone **2** was based on the internal cyclization of diynone (Scheme 2, Pathway 2). In this second strategy, the targeted intermediate was diynol **15**, which could be potentially synthesized from aldehyde **6** and alkyne **5c** (Scheme 5) and then oxidized in ketone and cyclized into **2**.

In this bottom-up approach, commercial propargyl alcohol (**8**) was easily protected as tetrahydropyranyl ether, compound **12**, with dihydropyrane (DHP) in CH_2Cl_2 and acidic

https://doi.org/10.1021/acs.joc.1c00598
J. Org. Chem. 2021, 86, 8112–8126

media.[24,25] Terminal alkyne was then alkylated with methyl iodide and *n*-BuLi (Scheme 5, compound **13**) and deprotected in the presence of *p*-TSA to give expected 2-butynyl alcohol **14**.[26] The last was oxidized with an excess of MnO_2 to afford corresponding 2-butynyl aldehyde **6**.[27] This aldehyde should have been coupled with terminal alkyne fragment-protected terminal alkyne **5c** to give diynol derivative **15**.[28,29] Unfortunately, in addition to partial polymerization (described as inevitable in the literature), aldehyde **6** oxidized into the corresponding carboxylic acid despite our various precautions (low temperature and dry and free oxygen conditions).[30] Thus, this strategy was not suitable for further developments.

Finally, diynol **15** was synthesized from guaiacol (**16**) according to the third retrosynthetic pathway (Scheme 2) *via* a top-down approach. After regioselective bromination with NBS (Scheme 6, compound **7**) and protection of phenolic function, MOM-protected bromoguaiacol was obtained with an overall yield of 90% (Scheme 6, compound **17**).[31−33] Then, Sonogashira coupling using propargyl alcohol (**8**) in the presence of palladium complex catalyst as well as copper cocatalyst led to butynyl alcohol derivative **18** in good yield.[34] The oxidation with an excess of manganese dioxide gave aldehyde **19** which did not exhibit the instability of **6**.[27,35] ynal **19** could undergo the addition of 1-propynylmagnesium bromide (**9**) to give expected aryl-hexa-1,4-diyn-3-ol **15** with a yield of 89%.[11] The last step before the cyclization in *γ*-pyrone was the oxidation of **15** to corresponding ketone **20** using MnO_2.[11,36] Thus, according to this synthetic way *γ*-pyrone's precursor **20** was obtained with an overall yield of 66%. Then, the cyclization of diynone **20** was performed *via* acid-mediated reaction (with triflic acid) in the presence of water, as previously described.[12] Target 2-aryl-*γ*-pyrone **2** was obtained with a good yield (52% in 7 steps) and was fully characterized by NMR, mass spectrometry, and elemental analysis.

To optimize the conditions of the aldolization/crotonization reaction between compounds **21** (MOM-protected *γ*-pyrone core) and **3c**, various parameters have been investigated, that is, the nature and quantity of the base, reaction time, and temperature (Scheme 7 and Table 1).[37,38]

Table 1. Influence of the Base, Time, and Temperature on the Reaction Yield and Stereoselectivity between Compounds 21 and 3c

entry	base	time (h)	*T* (°C)	yield (%)	*E*/*Z* molar ratio
1	NaOMe (1.2 equiv)	18	25	traces	n.d.
2	KOH (1.2 equiv)	18	25	**21** degradation	n.d.
3	NaOEt (1.2 equiv)	18	25	20	1/1
4	NaOEt (1.2 equiv)	48	40	38	95/5

On one side, only traces of alkene were obtained with solid sodium methanolate or potassium hydroxide, the latest even inducing the degradation of the pyrone cycle. On the other side, alkene was formed in moderate yield with freshly prepared sodium ethanolate. However, when the reaction was carried out at 25 °C for 18 h, the product was isolated with only a 20% yield and showed no stereoselectivity. An increase of the temperature to 40 °C and reaction time to 48 h was necessary to improve the conversion and to isolate after chromatography the product with a 38% yield. In these conditions, an enhancement of stereoselectivity was observed, isomer *E* being the major stereoisomer.

The optimized conditions (Table 1, line 4) were then used to couple protected aryl-*γ*-pyrone **21** (Scheme 7) with MOM-protected vanillin **3c**. Desired compound **22** was obtained with a 38% yield. Final acidic deprotection of aryl-*γ*-pyrone moieties afforded quasi-quantitatively target derivative **1**, an analogue of CC.[39] This newly reported compound was fully characterized by NMR and high-resolution mass spectrometry (HRMS) that confirmed the molecular structure.

2.3. Photophysical Properties of the 2,6-Disubstituted-*γ*-pyrone Analogue of CC, 1. *2.3.1. Simulated Absorption and Emission Spectra.* One-photon absorption spectrum was computed for comparison with the experiment. To that purpose, different DFT functionals and basis sets were benchmarked to characterize the excitation of the molecule; more details are provided in the ESI.

The CAM-B3LYP functional gave the best representation of the excited state manifold as compared to the other functional. This agreement holds despite a considerable shift in the absolute value of the absorption wavelengths that is common for range-separate functionals. It can be related to an improved representation of charge-transfer states compared to hybrid functionals that avoid the presence of significant intruder states, whose excitation energy would have been artificially lowered. Figure 2 shows the calculated absorption spectrum, taking into account the vibrational and dynamic effects modeled *via* a Wigner distribution sampling around the stationary minimum. Also, the emission spectrum was calculated by sampling the most stable minimum in the excited state in the gas phase. In the case of the absorption spectrum *in vacuo*, we observe an absorption maximum at around 310 nm, while the emission spectrum is considerably stoked-shifted peaking at 375 nm. Note also the important asymmetry of the absorption band due to the vibronic coupling and the large and rather shoulderless emission band. Both absorption and emission spectra match reasonably with the experimental ones, reported in the next section.

In conjunction with the gas phase exploration of the absorption and emissive properties, solvatochromism was investigated including the solvent effects implicitly via dielectric medium in the PCM approach (Figure 2 right). A slight red shift of the absorption maximum was observed when increasing the polarity of the solvent. Most remarkably, the spectrum in chloroform presents a noticeable shoulder at a wavelength higher than λ_{max}. The appearance of this feature might be due to the complex coupling between the electronic and nuclear degrees of freedom and most notably to the mixing of the lowest laying ($n-\pi^*$) and ($\pi-\pi^*$) states that are strongly dependent on the specific sampled geometry.

Moreover, the isomerization process was characterized by molecular modeling in a related publication.[40] It is shown that it occurs through the participation of $n-\pi^*$ and $\pi-\pi^*$ excited states. Notably, the process is more efficient than the one for natural CC due to the lower energy barriers found along the isomerization coordinates of both excited states' PESs. The more efficient isomerization can also explain the lower fluorescence quantum yield due to the triggering of a reactive dissociative channel.

2.3.2. Experimental Absorption and Emission Spectra. The photochromic properties of the 2,6-disubstituted-*γ*-pyrone

https://doi.org/10.1021/acs.joc.1c00598
J. Org. Chem. 2021, 86, 8112−8126

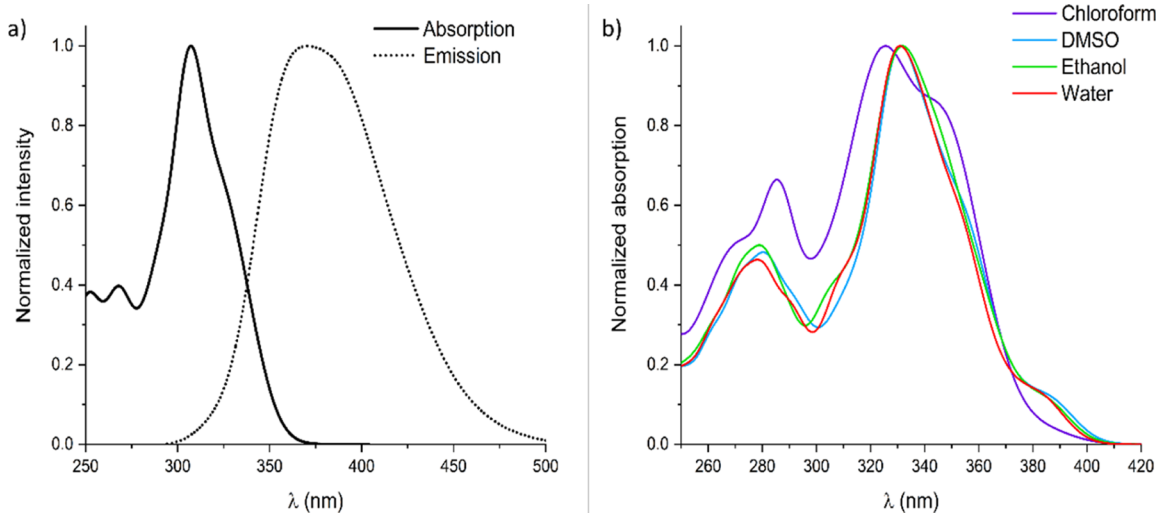

Figure 2. Absorption and emission spectra in the gas phase of 2,6-disubstituted-γ-pyrone analogue **1** at the CAM-B3LYP level (left). Absorption spectra in different solvents using the polarizable continuum model (PCM) (right).

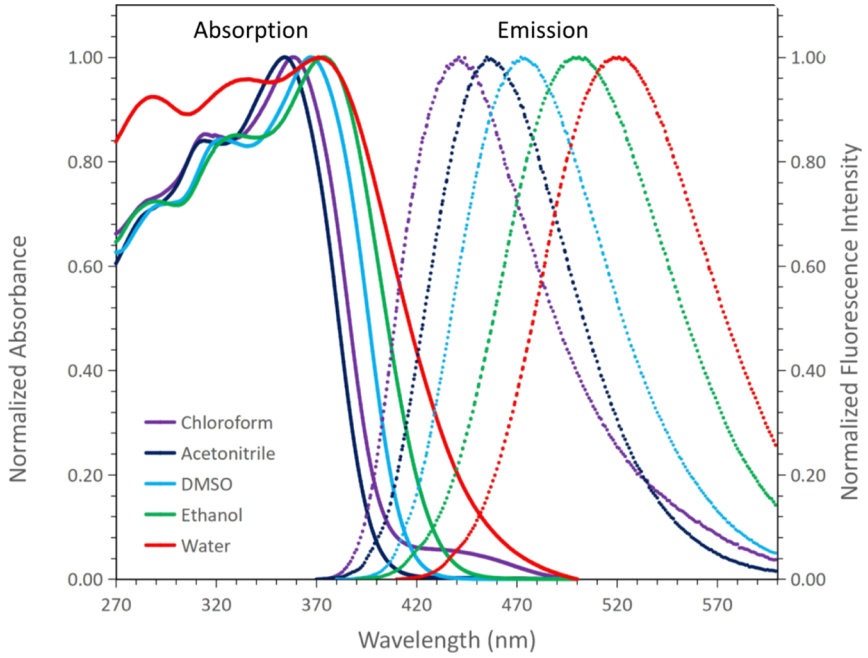

Figure 3. Normalized absorption (left) and emission (right) spectra of 2,6-disubstituted-γ-pyrone **1** upon excitation at λ_{max} in various solvents (at 358 nm in chloroform, 354 nm in acetonitrile, 367 nm in DMSO, 371 nm in ethanol, and 371 nm in water).

analogue of CC, **1**, were investigated in aprotic and protic solvents with various polarities (*i.e.*, $CHCl_3$, MeCN, DMSO, EtOH, and H_2O). The steady-state absorption spectra of pyrone at the ground state (GS) are shown in Figure 3 and correspond mainly to *E*-isomer as determined from NMR (Figure 5) (*E*/*Z* ratio of 100:0 in DMSO and 92:8 in EtOH). All spectra exhibit three broad absorption peaks, centered at—288, 327, and 374 nm in ethanol. The highest and the lowest energy absorption band were assigned to be mainly due to the $\pi-\pi^*$ transition of the phenyl-pyrone moiety ($D_1-\pi-A$) and the styryl-pyrone moiety ($A-\pi-D_2$), respectively (Figure 3), while the intermediate energy absorption band was assigned to the $n-\pi^*$ transition. The values related to the styryl-pyrone moiety are similar to the ones reported for CC, which exhibit in ethanol the main absorption peak at ∼370 nm and a shoulder peak at ∼330 nm.[3] This is consistent with the fact that the additional double bond in the pyran cycle is not inducing any extension of π-conjugation on the styryl-pyrone moiety ($A-\pi-D_2$) but rather an extension of planarity from one extreme to the other of the molecule (Figure 1).

An overall positive solvatochromism is observed which corresponds to a bathochromic shift (or red shift) with increasing solvent polarity. This could be due to a more important stabilization of the bright state ($\pi-\pi^*$) due to the higher dipolar moment of this excited state. The molar extinction coefficients (Table 2) at the respective maxima band also depend on the solvent; the highest value is obtained in MeCN (31,654 M^{-1} cm^{-1}) and the lowest in H_2O (14,632 M^{-1} cm^{-1}).

The fluorescence spectra of the 2,6-disubstituted-γ-pyrone analogue of CC were obtained upon excitation at the maxima band (358 nm in chloroform, 354 nm in acetonitrile, 367 nm

https://doi.org/10.1021/acs.joc.1c00598
J. Org. Chem. 2021, 86, 8112−8126

Table 2. Optical Properties of 2,6-Disubstituted-γ-pyrone 1 and Kinetics of the Photoisomerization Process

	$CHCl_3$	CH_3CN	DMSO	EtOH	H_2O
λ_{abs} (nm)	358	354	367	374	371
ε_E (M^{-1} cm^{-1})	27,000	31,654	27,927	27,220	14,632
λ_{em} (nm)	441	455	472	501	516
ϕ_F (%)	1.5	1.3	2.0	1.8	<1
E/Z (GS)[a]	n.d.	n.d.	100/0	92/8	n.d.
E/Z (PSS)[a]	n.d.	n.d.	47/53	25/75	n.d.
	$E \rightarrow Z$ at 25 °C, 375 nm[b]				
$k^{375}_{E\rightarrow Z} \times 10^3$ (s^{-1})	30	18	12	16	n.d.
$t^{375}_{1/2}$ (s)	23	39	58	43	n.d.
	$Z \rightarrow E$ at 25 °C, 300 nm[b]				
$k^{300}_{Z\rightarrow E} \times 10^3$ (s^{-1})	127	124	182	145	n.d.
$t^{300}_{1/2}$ (s)	5.5	5.6	3.8	4.8	n.d.
	$Z \rightarrow E$ Nonradiative (nr)[b]				
$k^{nr}_{Z\rightarrow E} \times 10^6$ (s^{-1}) at 25 °C[b]	1.6	<1	<1	4.4	n.d.
$t^{nr}_{1/2}$ (h) at 25 °C	120	>168	>168	44	n.d.
$k^{nr}_{Z\rightarrow E} \times 10^6$ (s^{-1}) at 40 °C[b]	38.9	2.7	14.7	5.3	n.d.
$t^{nr}_{1/2}$ (h) at 40 °C	5.0	71	13	36	n.d.

[a]As determined from NMR measurements. [b]As determined from UV−Vis measurements.

in DMSO, 371 nm in ethanol, and 371 nm in water) and are shown in Figure 3. Identical fluorescence spectra were obtained upon excitation at 320 nm in chloroform and acetonitrile and 330 nm in DMSO, ethanol, and water showing that the emission spectra do not depend on the excitation wavelength (Figure S3). Whatever the solvent, a broad fluorescence spectrum is observed, which is maximum Stokes shifted and increases with increasing solvent polarity. This indicates that the excited-state dipole moment of pyrone is significantly larger than that of its GS. Whatever the solvent, the quantum yields of fluorescence (ϕ) are low and do not exceed 2% (see Table 2). The lowest and the highest ϕ of 2,6-disubstituted-γ-pyrone were of 2% in DMSO and less than 1% in water, respectively. These values are much lower than those of CC, which has a fluorescence quantum yield of 9% in chloroform (*vs* 1.5% for the pyrone analogue) and 3% in acetonitrile (*vs* 1.3% for the pyrone analogue).[3]

The decrease in the fluorescence of 2,6-disubstituted-γ-pyrone **1** compared with CC could be attributed to the enhancement of nonradiative decay processes such as the excited-state isomerization of the styryl double bond. Moreover, this nonradiative deactivation process should be favored by the decrease of internal conversion of pyrone, more rigid and more planar than CC that can adopt several rotamer conformations. To further investigate this hypothesis, we characterize the photoisomerization process (Scheme 8) through combined steady-state absorption and NMR experiments.

2.3.3. Characterization of the Photoisomerization Efficiency. The isomerization of 2,6-disubstituted-γ-pyrone is a reversible process in which the direct isomerization consists of the photoinduced transformation of *E* into *Z*-isomer upon irradiation at a wavelength close to λ_{max} of *E*-isomer. The back switch represents the reverse reaction that takes place either by irradiation at 300 nm or thermally in the dark (Scheme 8). This process can be followed either by monitoring the time evolution of the UV/Vis absorption spectrum and, in particular, of the intensity of the signature 370 and 300 nm bands (Figure 4) or the modification in the chemical shifts on the ^{1}H NMR spectra (Figure 5).

At first, NMR experiments were performed to characterize both the GS and the PSS. Full NMR spectra and peak positions of 2,6-disubstituted-γ-pyrone 1 are provided in the Supporting Information. While *E*-form is the thermodynamically favored isomer, the interconversion into *Z* can be induced upon irradiation at a wavelength close to the maximum absorption band of about 370 nm. Figure 5 shows the most important changes in the ^{1}H NMR spectrum observed between the GS and the PSS in ethanol-d_6 and DMSO-d_6. For instance, in DMSO, the protons of *E*-form of the styryl moiety were assigned at 7.52 (H^E_β) and 7.01 (H^E_α) and the protons of *Z*-form at 6.94 (H^Z_β) and 6.32 ppm (H^Z_α). These protons can be easily identified because the vicinal coupling constants are always larger for *E*-isomers (J_{HH} = 12−18 Hz, herein: 16.1 Hz) than for *Z*-isomers (J_{HH} = 0−12 Hz, herein: 12.1 Hz). As a general trend, the intensity of the protons of the *E* styryl moiety is decreasing upon excitation at 375 nm. However, they appear within a multiplet, and therefore, the accurate quantification of the *E*/*Z* ratio, via the peak integrals is rather cumbersome. Hence, we instead quantified the protons belonging to the two $-OCH_3$ groups appearing at 3.94 and 3.89 for *E* isomer and at 3.62 and 3.56 for *Z*-isomer that are perfectly resolved and not overlapping (Figure 5). As indicated in Table 2, upon irradiation at λ_{max}, the *E*/*Z* ratio changed from 100/0 to 47/53 in DMSO and from 92/8 to 25/75 in ethanol. Interestingly, upon irradiation at 300 nm, the reverse, switch back process was not complete and yielded an *E*/*Z* ratio of 64/36 in both DMSO and ethanol. Moreover, the photoisomerization was perfectly reversible for at least five cycles under consecutive irradiation at 375 or 300 nm (Figure 6, left) and occurred within several minutes despite the moderate power of the LEDs used as the illumination source (see Experimental Section: kinetics and Figures 6 right and S4 and S5).

Scheme 8. Reversible *E*/*Z* Photoisomerization Scheme of Quadrupolar Compound 1 Showing Direct Isomerization upon Irradiation at 375 nm and Reverse Reaction Taking Place Either by Irradiation at 300 nm or Thermally in the Dark

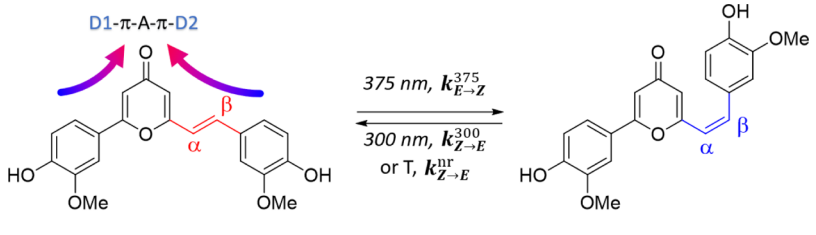

1 (*E*) 1 (*Z*)

https://doi.org/10.1021/acs.joc.1c00598
J. Org. Chem. 2021, 86, 8112−8126

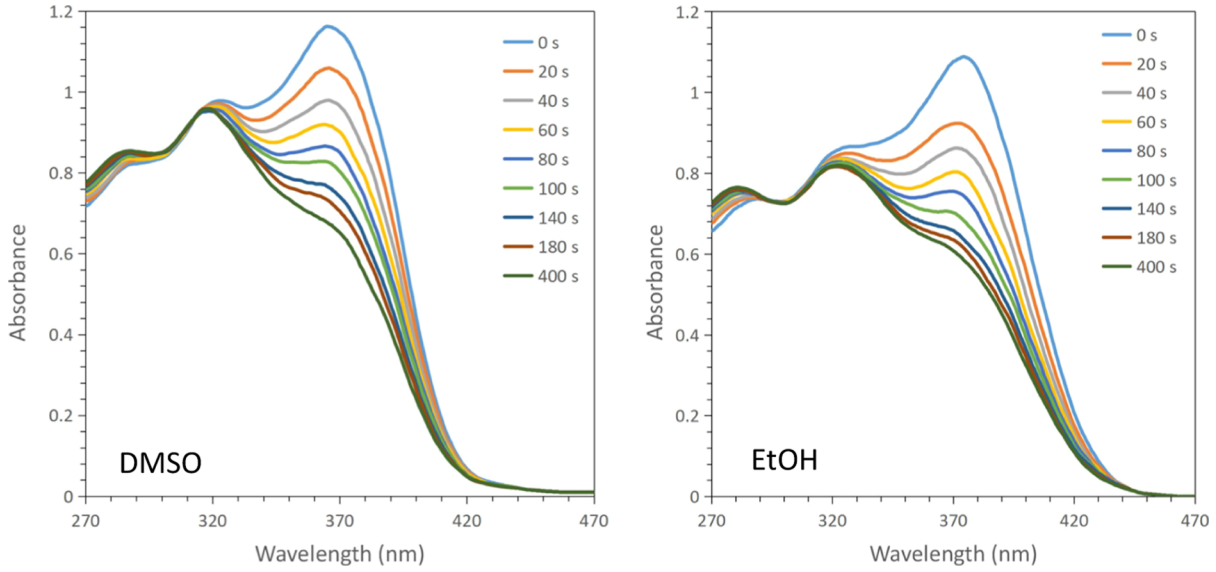

Figure 4. Spectral evolution of the $E \rightarrow Z$ photoisomerization from the GS to the photostationary state (PSS), upon irradiation at 375 nm in DMSO (left) and in ethanol (right).

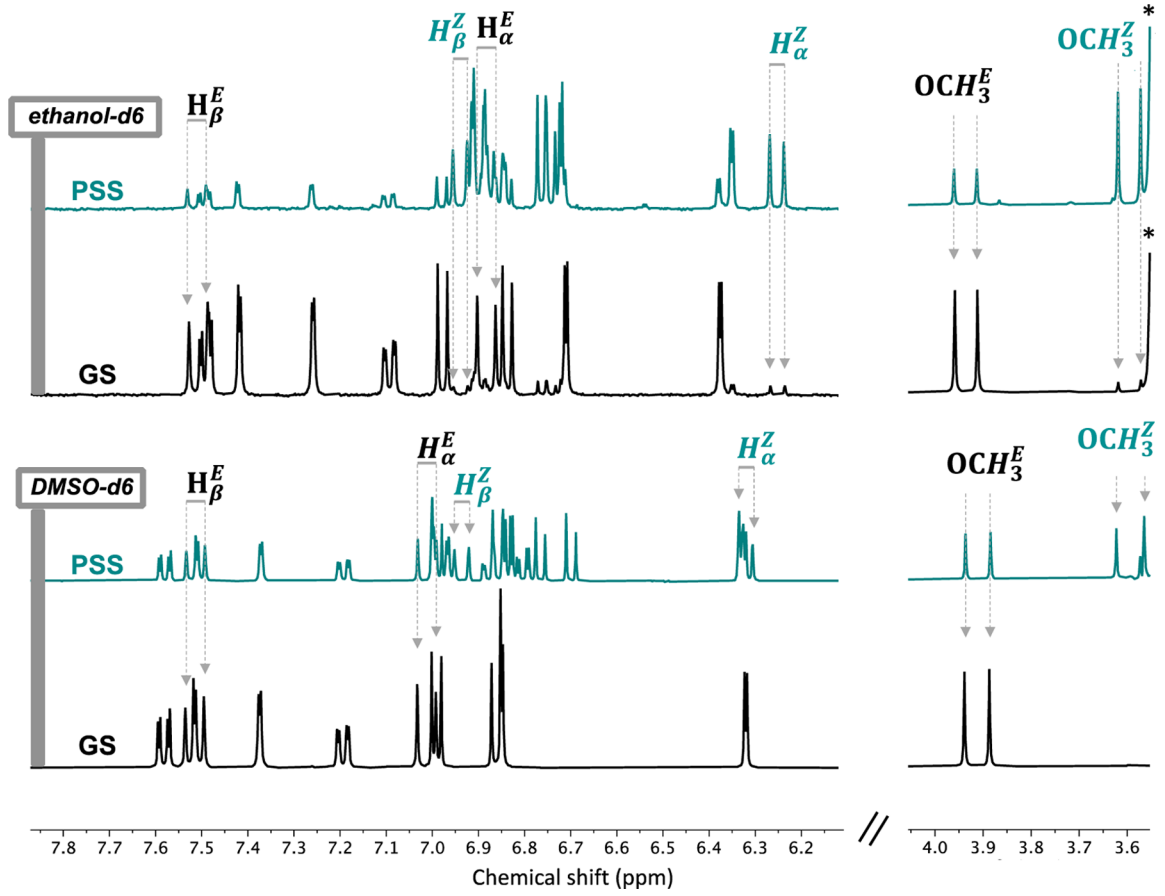

Figure 5. Representative ^{1}H NMR spectra of 2,6-disubstituted-γ-pyrone **1** in ethanol-d_6 and DMSO-d_6 at both the GS (black line) and the PSS (cyan line).

Figure 4 shows a typical evolution of the absorption band of 2,6-disubstituted-γ-pyrone upon irradiation at 375 nm in EtOH and DMSO. Additional UV spectra of the direct and reverse switch in chloroform and acetonitrile are given in the Supporting Information. From the kinetic profiles of the direct and reverse switch (Figure 6 right), one can determine the kinetic parameters such as isomerization half-life times and rate constants (Table 2). It was observed that the rate constant of the direct $E \rightarrow Z$ switch decreases with increasing polarity of the solvent, from 30×10^{-3} s^{-1} in chloroform to 16×10^{-3} s^{-1} in ethanol, except for DMSO, more viscous, for which $k_{E\rightarrow Z}^{375} = 12 \times 10^{-3}$ s^{-1}. On the contrary, the highest rate constant of the

https://doi.org/10.1021/acs.joc.1c00598
J. Org. Chem. 2021, 86, 8112−8126

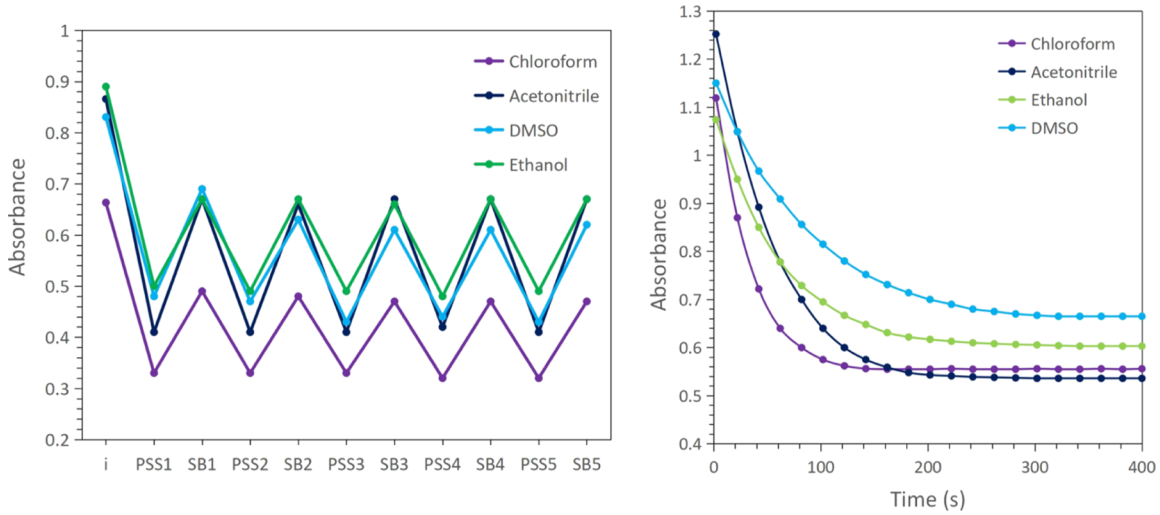

Figure 6. Absorption changes at λ_{max} during the successive irradiation at two different wavelengths, 375 and 300 nm (left) and during the $E \rightarrow Z$ photoisomerization process at 375 nm as a function of time (right).

reverse reaction, under irradiation at 300 nm, was obtained in DMSO, $k^{300}_{Z\rightarrow E} = 182 \times 10^{-3}$ s^{-1}. On the other side, the thermal back switch was extremely slow $k^{nr}_{Z\rightarrow E} < 1 \times 10^{-6}$ s^{-1} at 25 °C and only increases slightly to $k^{nr}_{Z\rightarrow E} = 14.7 \times 10^{-6}$ s^{-1} at 40 °C (Figure S6). This negligible thermal switch is of paramount importance for high temporal control of the switch, only triggered by irradiation.

3. CONCLUSIONS

In summary, we designed and synthesized a 2,6-disubstituted-γ-pyrone analogue of CC, a natural photoswitch in the UV−Vis region, in order to improve its photophysical properties and more particularly to increase the cross-section value of TPA.[41] Indeed, this feature is compulsory for further *in vivo* applications for which irradiation in the NIR region is needed. To do so, three retrosynthetic pathways were explored. While the passage through an isoxazole intermediate could have been more straightforward and could provide the target final molecule in only 5 steps instead of 10; the corresponding yields were too low (<30%). Therefore, the pathway involving the cyclization of diynone was preferred. In this case, we showed that the choice of the starting substrate, guaiacol versus propargyl alcohol, is of paramount importance as is conditioning the formation of highly reactive and volatile intermediates such as 2-butynyl aldehyde, if propargyl alcohol is used. Thus, diynone was built step-by-step, through a bottom-up approach from guaiacol, followed by its cyclization and by the formation of the carbon−carbon double bond *via* aldolization/crotonization reaction on residual methylene of the preformed pyrone ring. Finally, it was shown that the isomerization of the resulted analogue is a reversible process in which (i) the direct isomerization consists of the transformation of *E*-pyrone into *Z*-pyrone upon irradiation at 375 nm, and (ii) the back switch is the reverse reaction that takes place either by irradiation at 300 nm or thermally, in the dark. The 2,6-disubstituted-γ-pyrone analogue of CC showed excellent photoswitching properties, low fatigue over at least five cycles, and better stability compared to CC. Due to the planar pyrone moiety of the quadrupolar D−π−A−π−D system, the value of the two-photon cross-section (159 GM) was higher than the one of CC (14 GM), as estimated from DFT calculations. Moreover, we have shown that, different from CC, photoswitching occurs with significant yields rather independently from the solvent polarity. Hence, we believe that our molecular design has tuned the competition between the different relaxation pathways favoring isomerization over fluorescence. Altogether our results indicate that our designed compound is of interest for further applications as a molecular photoswitch activable via TPA excitation, and hence, could be potentially used in the biomedical field.

4. EXPERIMENTAL SECTION

4.1. General. All reactions were carried out under an argon atmosphere. Toluene and THF were dried using a MBRAUN MB-SPS-800 solvent purification system. Other solvents and liquid reagents were purified and dried according to recommended procedures. The chemical reagents were purchased from Merck, Fisher Scientific, or Sigma-Aldrich and were used as received. Analytical TLC analyses were performed using standard procedures on silica gel 60 F254 plates (Merck). The compounds were visualized with UV light (254 nm), and alternatively, potassium permanganate aqueous solution was used. Silica gel column chromatography was performed on a glass column filled with silica gel (63−200 μm) (Merck). The melting points (mp) were determined with a Tottoli apparatus and are uncorrected. Spectroscopic analyses and kinetic measurements were carried out on the PhotoNS Platform of the L2CM Laboratory, University of Lorraine. FTIR spectra were recorded on a Shimadzu IRAffinity-1 apparatus equipped with ATR PIKE Technologies model GladiATR (cm^{-1}). NMR spectra were recorded at 300 K, unless stated otherwise, using a Bruker DRX400 spectrometer (400 MHz for ^{1}H and 100.6 MHz for ^{13}C). Chemical shifts are reported in ppm (δ) relative to deuterated solvent residual peaks. For complete assignment of ^{1}H and ^{13}C signals, two-dimensional ^{1}H, ^{1}H COSY and ^{1}H, ^{13}C correlation spectra were recorded. The following abbreviations are used to explain the observed multiplicities: s, singlet; d, doublet; dd, doublet of doublets; ddd, doublet of doublets of doublets; t, triplet; td, triplet of doublets; m, multiplet; and bs, broad singlet. HRMS were recorded on a microTOFQ (Bruker) ESI/QqTOF spectrometer. The compounds **3b**, **3c**, **4**, **5b**, and **10b** used in the first pathway were synthesized according to the methods reported in refs 18 19 21 42, and 43, respectively. According to the second pathway, compounds **12**, **13**, and **14** were obtained by following ref 26 and derivative **6** according to ref 27. Compounds **7** and **17** used in the third pathway were synthesized according to the methods described in refs 32 and 33, respectively.

https://doi.org/10.1021/acs.joc.1c00598
J. Org. Chem. 2021, 86, 8112−8126

4.2. Synthesis. *4.2.1. 4-(2,2-Dibromovinyl)-2-methoxyphenol, **10a**.* To a stirred solution of vanillin **3a** (2.05 g, 13.44 mmol) and CBr_4 (8.95 g, 26.98 mmol, 2.0 equiv) in dry DCM (40 mL) at 0 °C was added fractionally PPh_3 (14.21 g, 54.19 mmol, 4.0 equiv). The mixture was further stirred for 3 h at 0 °C (CCM, SiO_2, and cyclohexane/EtOAc, 85:15). The reaction mixture was quenched with water (30 mL), and the organic phase was separated. The aqueous phase was further extracted with DCM (3 × 30 mL). The combined organic phases were washed with water (3 × 30 mL) and brine (3 × 30 mL) and then dried over Na_2SO_4, filtered, and evaporated under reduced pressure. Purification by chromatography (SiO_2 and Cyclohexane/EtOAc, 85:15) afforded compound **10a** as a yellow oil (4.12 g, 99%). R_f: 0.38 (cyclohexane/EtOAc, 85:15); ^{1}H NMR (400 MHz, $CDCl_3$): δ 7.39 (s, 1H; Ar-C*H*), 7.19 (d, $J_{H,H}$ = 1.8 Hz, 1H; Ar-*H*), 7.04 (dd, $J_{H,H}$ = 8.3, 1.9 Hz; Ar-*H*), 6.91 (d, $J_{H,H}$ = 8.2 Hz, 1H; Ar-*H*), 5.85 (s, 1H; O*H*), 3.89 (s, 3H; OCH_3); ^{13}C{^{1}H} NMR (100 MHz, $CDCl_3$): δ 146.3, 146.2, 136.6, 127.5, 122.8, 114.4, 110.6, 87.2, 56.1. ESI-MS (HR) *m*/*z*: $[M + Na]^+$ calcd for $C_9H_8{}^{79}Br_2NaO_2$, 328.8783; found, 328.8784.

*4.2.2. 4-(2,2-Dibromovinyl)-2-methoxy-1-(methoxymethoxy)-benzene, **10c**.* To a stirred solution of 3-methoxy-4-(methoxymethoxy)benzaldehyde **3c** (503 mg, 2.56 mmol) and CBr_4 (1.72 g, 5.19 mmol, 2.0 equiv) in dry DCM (50 mL) at 0 °C was added PPh_3 (2.71 g, 10.33 mmol, 4.0 equiv) fractionally, and the mixture was stirred 3 h at 0 °C (CCM, SiO_2, and cyclohexane/EtOAc 95:5). The reaction mixture was quenched with water (30 mL), and the organic phase was separated. The aqueous phase was further extracted with DCM (3 × 30 mL). The combined organic phase was washed with water (3 × 30 mL) and brine (3 × 30 mL) and then dried over Na_2SO_4, filtered, and evaporated under reduced pressure. Chromatography on silica gel with EtOAc (2%) in cyclohexane afforded title compound **10c** as a yellow oil (675 mg, 75%). R_f: 0.29 (cyclohexane/EtOAc 95:5). ^{1}H NMR (400 MHz, $CDCl_3$): δ 7.41 (s, 1H; Ar-C*H*), 7.19 (d, $J_{H,H}$ = 1.3 Hz, 1H; Ar-*H*), 7.06 (d, $J_{H,H}$ = 8.4 Hz, 1H; Ar-*H*), 7.04 (dd, $J_{H,H}$ = 8.4, 1.3 Hz, 1H; Ar-*H*), 5.24 (s, 2H; OCH_2O), 3.88 (s, 3H; OCH_3), 3.51 (s, 3H; OCH_3). ^{13}C{^{1}H} NMR (100 MHz, $CDCl_3$): δ 149.4, 146.9, 136.5, 129.6, 122.0, 115.9, 111.8, 95.4, 88.1, 56.4, 56.1. ESI-MS (HR) *m*/*z*: $[M + H]^+$ calcd for $C_{11}H_{13}{}^{79}Br_2O_3$, 350.9226; found, 350.9236; *m*/*z*: $[M + Na]^+$ calcd for $C_{11}H_{12}{}^{79}Br_2NaO_3$, 372.9045; found, 372.9053.

*4.2.3. 4-Ethynyl-2-methoxyphenol, **5a**.* To a stirred solution of 4-(2,2-dibromovinyl)-2-methoxyphenol **10a** (3.00 g, 9.73 mmol) in dry THF (100 mL) at −78 °C was added *n*-BuLi (1.4 M in THF, 28 mL, 39.20 mmol, 4.0 equiv) dropwise, and the mixture was stirred 3 h at −78 °C (CCM, SiO_2, and cyclohexane/EtOAc 85:15). The reaction mixture was quenched with NH_4Cl (70 mL), and the organic phase was separated. The aqueous phase was further extracted with DCM (3 × 50 mL). The combined organic phase was washed with water (3 × 50 mL) and brine (3 × 50 mL) and then dried over Na_2SO_4, filtered, and evaporated under reduced pressure. Chromatography on silica gel with EtOAc (15%) in cyclohexane afforded title compound **5a** as a brown oil (1.27 g, 88%). ^{1}H NMR (400 MHz, $CDCl_3$): δ 7.06 (dd, $J_{H,H}$ = 8.2, 1.7 Hz, 1H; Ar-*H*), 6.98 (d, $J_{H,H}$ = 1.6 Hz, 1H; Ar-*H*), 6.86 (d, $J_{H,H}$ = 8.2 Hz, 1H; Ar-*H*), 5.83 (s, 1H; O*H*), 3.87 (s, 3H; OCH_3), 2.99 (s, 1H; C*H*). The NMR data are in agreement with the literature.[44]

*4.2.4. 4-Ethynyl-2-methoxy-1-(methoxymethoxy)benzene, **5c**.* To a stirred solution of 4-(2,2-dibromovinyl)-2-methoxy-1-(methoxymethoxy)benzene **10c** (150 mg, 0.43 mmol) in dry THF (30 mL) at −78 °C was added *n*-BuLi (1.4 M in THF, 0.8 mL, 1.12 mmol, 2.6 equiv) dropwise, and the mixture was stirred 3 h at −78 °C (CCM, SiO_2, and cyclohexane/EtOAc 9:1). The reaction mixture was quenched with NH_4Cl (20 mL), and the organic phase was separated. The aqueous phase was further extracted with DCM (3 × 20 mL). The combined organic phase was washed with water (3 × 20 mL) and brine (3 × 20 mL) and then dried over Na_2SO_4, filtered, and evaporated under reduced pressure. Chromatography on silica gel with EtOAc (10%) in cyclohexane afforded title compound **5c** as a yellow oil (79 mg, 95%). R_f: 0.32 (cyclohexane/EtOAc 9:1). ^{1}H NMR (400 MHz, $CDCl_3$): δ 7.09−7.05 (m, 2H; Ar-*H*), 7.01 (m, 1H; Ar-*H*), 5.23 (s, 2H; OCH_2O), 3.87 (s, 3H; OCH_3), 3.50 (s, 3H; OCH_3), 3.01 (s, 1H; C*H*). ^{13}C{^{1}H} NMR (100 MHz, $CDCl_3$): δ 149.5, 147.5, 125.6, 116.1, 116.0, 115.5, 95.5, 83.8, 76.1, 56.4, 56.1. ESI-MS (HR) *m*/*z*: $[M + H]^+$ calcd for $C_{11}H_{13}O_3$, 193.0859; found, 193.0841; *m*/*z*: $[M + Na]^+$ calcd for $C_{11}H_{12}NaO_3$, 215.0679; found, 215.0670.

*4.2.5. 3-(3-Methoxy-4-(methoxymethoxy)phenyl)prop-2-yn-1-ol, **18**.* To a stirred solution of 4-bromo-2-methoxy-1-(methoxymethoxy)benzene **17** (3.80 g, 15.39 mmol) in diisopropylamine (^{i}Pr_2NH, 80 mL) were added $PdCl_2(PPh_3)_2$ (0.22 g, 0.32 mmol, 0.02 equiv), CuI (0.12 g, 0.62 mmol, 0.04 equiv), and PPh_3 (0.16 g, 0.62 mmol, 0.04 equiv). The solution was extensively degassed by argon bubbling. Propargyl alcohol (**8**) (1.20 mL, 20.32 mmol, 1.32 equiv) was added, and the mixture was stirred overnight at 80 °C with a heating mantle (CCM, SiO_2, cyclohexane/EtOAc, 3:1). After cooling and filtration on a short pad of silica gel eluted with EtOAc, the resulting filtrate was washed with water (3 × 50 mL) and brine (3 × 50 mL) and then dried over Na_2SO_4, filtered, and purified by chromatography (SiO_2 and cyclohexane/EtOAc, 8:2 to 1:1) to afford compound **18** as a brown oil (3.14 g, 92%). R_f: 0.27 (cyclohexane/EtOAc, 1:1). IR (ATR, cm^{-1}) ν: 3385 (OH), 2230. ^{1}H NMR (400 MHz, $CDCl_3$): δ 7.08 (d, $J_{H,H}$ = 8.3 Hz, 1H; Ar-*H*), 7.00 (dd, $J_{H,H}$ = 8.3, 1.8 Hz, 1H; Ar-*H*), 6.97 (d, $J_{H,H}$ = 1.8 Hz, 1H; Ar-*H*), 5.23 (s, 2H; OCH_2O), 4.49 (d, $J_{H,H}$ = 4.8 Hz, 2H; CH_2), 3.87 (s, 3H; OCH_3), 3.51 (s, 3H; OCH_3), 2.27 (br s, 1H; O*H*). ^{13}C{^{1}H} NMR (100 MHz, $CDCl_3$): δ 149.4, 147.1, 125.0, 116.5, 116.0, 115.0, 95.4, 86.3, 85.5, 56.4, 56.0, 51.6. ESI-MS (HR) *m*/*z*: $[M + H]^+$ calcd for $C_{12}H_{15}O_4$, 223.0965; found, 223.0974; *m*/*z*: $[M + Na]^+$ calcd for $C_{12}H_{14}NaO_4$, 245.0784; found, 245.0795.

*4.2.6. 3-(3-Methoxy-4-(methoxymethoxy)phenyl)-propiolaldehyde, **19**.* A suspension of MnO_2 (11.80 g, 0.136 mol, 10 equiv) in dry DCM (120 mL) was added to 3-(3-methoxy-4-(methoxymethoxy)phenyl)prop-2-yn-1-ol **18** (3.02 g, 13.61 mmol) and stirred overnight at room temperature (CCM, SiO_2, cyclohexane/EtOAc, 3:1). Filtration on a short pad of silica gel eluted with DCM gave a filtrate which was concentrated and chromatographed (SiO_2 and cyclohexane/EtOAc, 75:25) to afford compound **19** as a brown oil (2.79 g, 93%). R_f: 0.37 (cyclohexane/EtOAc, 3:1). IR (ATR, cm^{-1}): 2176, 1647 (CH═O). ^{1}H NMR (400 MHz, $CDCl_3$): δ 9.39 (s, 1H; C*H*O), 7.22 (dd, $J_{H,H}$ = 8.4, 1.9 Hz, 1H; Ar-*H*), 7.15 (d, $J_{H,H}$ = 8.4 Hz, 1H; Ar-*H*), 7.11 (d, $J_{H,H}$ = 1.8 Hz, 1H; Ar-*H*), 5.28 (s, 2H; OCH_2O), 3.89 (s, 3H; OCH_3), 3.51 (s, 3H; OCH_3). ^{13}C{^{1}H} NMR (100 MHz, $CDCl_3$): δ 176.8, 149.8, 149.6, 127.7, 116.2, 115.8, 112.8, 96.3, 95.3, 88.5, 56.6, 56.2. ESI-MS (HR) *m*/*z*: $[M + H]^+$ calcd for $C_{12}H_{13}O_4$, 221.0808; found, 221.0802; *m*/*z*: $[M + Na]^+$ calcd for $C_{12}H_{12}NaO_4$, 243.0628; found, 243.0631.

*4.2.7. 1-(3-Methoxy-4-(methoxymethoxy)phenyl)hexa-1,4-diyn-3-ol, **15**.* To a solution of 3-(3-methoxy-4-(methoxymethoxy)-phenyl)propiolaldehyde **19** (0.33 g, 1.50 mmol) in anhydrous THF (5 mL) was added 1-propynylmagnesium bromide (**9**) (0.50 M solution in THF, 4.50 mL, 2.25 mmol, 1.50 equiv) at −20 °C and stirred for 0.5 h. Stirring was maintained for another 1 h at room temperature (CCM, SiO_2, and cyclohexane/EtOAc, 4:1). The reaction mixture was then quenched with saturated aqueous NH_4Cl (3 mL), and the organic phase was separated. The aqueous phase was further extracted with DCM (3 × 5 mL), and the combined organic phases were washed with water (3 × 5 mL) and brine (3 × 5 mL) and then dried over Na_2SO_4 and filtered. The concentrated filtrate was purified by chromatography (SiO_2 and cyclohexane/EtOAc, 8:2 to 1:1) to afford diynol **15** as a yellow oil (0.347 g, 89%). R_f: 0.22 (cyclohexane/EtOAc, 4:1). IR (ATR, cm^{-1}): 3354 (OH), 2181. ^{1}H NMR (400 MHz, $CDCl_3$): δ 7.06 (d, $J_{H,H}$ = 8.3 Hz, 1H; Ar-*H*), 7.01 (dd, $J_{H,H}$ = 8.3, 1.8 Hz, 1H; Ar-*H*), 6.98 (d, $J_{H,H}$ = 1.7 Hz, 1H; Ar-*H*), 5.30 (br s, 1H; O*H*), 5.22 (s, 2H; OCH_2O), 3.85 (s, 3H; OCH_3), 3.49 (s, 3H; OCH_3), 2.52 (d, $J_{H,H}$ = 5.0 Hz, 1H; C*H*), 1.88 (d, $J_{H,H}$ = 2.2 Hz, 3H; CH_3). ^{13}C{^{1}H} NMR (100 MHz, $CDCl_3$): δ 149.4, 147.5, 125.3, 116.0, 115.9, 115.2, 95.5, 85.5, 84.1, 83.3, 81.6, 56.5, 56.1, 53.0, 3.9. ESI-MS (HR) *m*/*z*: $[M + H]^+$ calcd for $C_{15}H_{17}O_4$, 261.1121; found, 261.1136; *m*/*z*: $[M + Na]^+$ calcd for $C_{15}H_{16}NaO_4$, 283.0941; found, 283.1018.

https://doi.org/10.1021/acs.joc.1c00598
J. Org. Chem. 2021, 86, 8112−8126

*4.2.8. 1-(3-Methoxy-4-(methoxymethoxy)phenyl)hexa-1,4-diyn-3-one, **20**.* MnO_2 (9.49 g, 0.109 mol, 20 equiv) was added into a solution of 1-(3-methoxy-4-(methoxymethoxy)-phenyl)-propiolaldehyde **15** (1.41 g, 5.43 mmol) in dry DCM (50 mL). The mixture was stirred overnight at room temperature (CCM, SiO_2, and cyclohexane/EtOAc, 4:1). The reaction mixture was then filtered on a short pad of silica gel eluted with DCM, and the resulting filtrate was concentrated and purified by chromatography (SiO_2 and cyclohexane/EtOAc, 85:25) to give diynone **20** as a brown oil (1.36 g, 97%). R_f: 0.31 (cyclohexane/EtOAc, 4:1). IR (KBr): 2181, 1616 (C═O). ^{1}H NMR (400 MHz, $CDCl_3$): δ 7.23 (dd, $J_{H,H}$ = 8.4, 1.9 Hz, 1H; Ar-*H*), 7.14 (d, $J_{H,H}$ = 8.4 Hz, 1H; Ar-*H*), 7.12 (d, $J_{H,H}$ = 1.8 Hz, 1H; Ar-*H*), 5.28 (s, 2H; OCH_2O), 3.89 (s, 3H; OCH_3), 3.51 (s, 3H; OCH_3), 2.10 (s, 3H; CH_3). ^{13}C{^{1}H} NMR (100 MHz, $CDCl_3$): δ 161.0, 149.7, 149.5, 127.8, 116.0, 115.7, 112.8, 95.3, 91.6, 91.4, 89.3, 81.6, 56.6, 56.2, 4.5. ESI-MS (HR) *m/z*: $[M + H]^+$ calcd for $C_{15}H_{15}O_4$, 259.0965; found, 259.0979; *m/z*: $[M + Na]^+$ calcd for $C_{15}H_{14}NaO_4$, 281.0784; found, 281.0807.

*4.2.9. 2-(4-Hydroxy-3-methoxyphenyl)-6-methyl-4H-pyran-4-one, **2**.* TfOH (2.4 μL, 27.12 mmol, 1.0 equiv) was added dropwise to a solution of 1-(3-methoxy-4-(methoxymethoxy)phenyl)hexa-1,4-diyn-3-one **20** in deionized water (77 mL), and the mixture was stirred 4 h at 100 °C with a heating mantle (CCM, SiO_2, EtOAc/MeOH, 9:1). After cooling to room temperature, the reaction mixture was diluted with water (20 mL) and EtOAc (20 mL). The organic phase was separated, and the aqueous phase was further extracted with EtOAc (3 × 20 mL). The combined organic phases were washed with water (3 × 20 mL) and brine (3 × 20 mL) and then dried over Na_2SO_4 and filtered. The filtrate was chromatographed (SiO_2 and EtOAc/MeOH, 9:1) and afforded compound **2** as a white solid (4.95 g, 79%). R_f: 0.34 (EtOAc/MeOH, 9:1). mp 112 °C. IR (ATR, cm^{-1}): 3410, 1651, 1645, 1520, 856. UV−Vis (DMSO): 316 nm. ^{1}H NMR (400 MHz, $CDCl_3$): δ 7.33 (dd, $J_{H,H}$ = 8.4, 2.1 Hz, 1H; Ar-*H*), 7.19 (d, $J_{H,H}$ = 2.1 Hz, 1H; Ar-*H*), 7.00 (d, $J_{H,H}$ = 8.4 Hz, 1H; Ar-*H*), 6.62 (d, $J_{H,H}$ = 2.2 Hz, 1H; H_{pyrone}), 6.17 (dd, $J_{H,H}$ = 2.0, 0.6 Hz, 1H; H_{pyrone}), 3.95 (s, 3H; OCH_3), 2.37 (d, $J_{H,H}$ = 0.5 Hz, 3H; CH_3). ^{13}C{^{1}H} NMR (100 MHz, $CDCl_3$): δ 180.6, 165.4, 164.0, 149.1, 147.2, 123.4, 120.2, 115.2, 114.2, 109.5, 108.2, 56.2, 20.0. ESI-MS (HR) *m/z*: $[M + H]^+$ calcd for $C_{13}H_{13}O_4$, 233.0808; found, 233.0812.

*4.2.10. 2-(3-Methoxy-4-(methoxymethoxy)phenyl)-6-methyl-4H-pyran-4-one, **21**.* To a solution of 2-(4-hydroxy-3-methoxyphenyl)-6-methyl-4*H*-pyran-4-one **2** (40 mg, 0.17 mmol) in DCM (5 mL) were added DIPEA (67 μL, 0.26 mmol, 1.50 equiv) and MOM chloride (20 μL, 0.38 mmol, 2.21 equiv) under stirring at 0 °C. After addition, the flask was sealed, and the mixture was stirred for 3 h at room temperature (CCM, SiO_2, and EtOAc). The reaction mixture was quenched with saturated aqueous NH_4Cl (3 mL), and the organic phase was separated. The aqueous phase was further extracted with DCM (3 × 5 mL). The combined organic phases were washed with water (3 × 5 mL) and brine (3 × 5 mL) and then dried over Na_2SO_4, filtered, concentrated, and purified by chromatography (SiO_2 and EtOAc) to afford protected derivative **21** as a white solid (47 mg, 98%). R_f: 0.30 (EtOAc). mp 158 °C. IR (ATR, cm^{-1}): 1655, 1612, 1512, 858. UV−Vis (DMSO): 310 nm. ^{1}H NMR (400 MHz, $CDCl_3$): δ 7.29 (dd, $J_{H,H}$ = 8.5, 2.2 Hz, 1H; Ar-*H*), 7.19 (d, $J_{H,H}$ = 2.1 Hz, 1H; Ar-*H*), 7.17 (d, $J_{H,H}$ = 8.5 Hz, 1H; Ar-*H*), 6.57 (d, $J_{H,H}$ = 2.2 Hz, 1H; H_{pyrone}), 6.10 (dd, $J_{H,H}$ = 2.1, 0.7 Hz, 1H; H_{pyrone}), 5.23 (s, 2H; OCH_2O), 3.89 (s, 3H; OCH_3), 3.47 (s, 3H; OCH_3), 2.32 (d, $J_{H,H}$ = 0.6 Hz, 3H; CH_3). ^{13}C{^{1}H} NMR (100 MHz, $CDCl_3$): δ 180.2, 165.2, 163.4, 149.9, 149.2, 125.3, 119.2, 115.9, 114.2, 109.9, 109.0, 95.2, 56.4, 56.1, 19.9. ESI-MS (HR) *m/z*: $[M + H]^+$ calcd for $C_{15}H_{17}O_5$, 277.1071; found, 277.1088; *m/z*: $[M + Na]^+$ calcd for $C_{15}H_{16}NaO_5$, 299.0890; found, 299.0899.

*4.2.11. (E)-2-(3-Methoxy-4-(methoxymethoxy)phenyl)-6-(3-methoxy-4-(methoxymethoxy)styryl)-4H-pyran-4-one, **22**.* A freshly prepared NaOEt solution (1.478 M in EtOH, 2.2 mL, 3.25 mmol, 1.79 equiv) was added dropwise to a mixture of 2-(3-methoxy-4-(methoxymethoxy)phenyl)-6-methyl-4*H*-pyran-4-one **21** (500 mg, 1.81 mmol) and 3-methoxy-4-(methoxymethoxy)benzaldehyde **3c** (510 mg, 2.59 mmol, 1.43 equiv) in dry EtOH (20 mL) at room temperature. Then, the mixture was warmed to 40 °C with a heating mantle and stirred for 48 h (CCM, SiO_2, and EtOAc). The reaction was quenched with water (10 mL), and the crude product was extracted with DCM (4 × 10 mL). The combined organic phases were washed with water (3 × 10 mL) and brine (3 × 10 mL) and then dried over Na_2SO_4 and filtered. The concentrated filtrate was purified by column chromatography (SiO_2 and EtOAc) to give title compound **22** as a yellow solid (310 mg, 38%). R_f: 0.28 (EtOAc). mp 131 °C. IR (ATR, cm^{-1}): 3076, 2932, 1645, 1628, 1599, 1504. UV−Vis (DMSO): 356 nm. ^{1}H NMR (400 MHz, $CDCl_3$): δ 7.46 (dd, $J_{H,H}$ = 8.5, 2.0 Hz, 1H; Ar-*H*), 7.42 (d, $J_{H,H}$ = 16.0 Hz, 1H; H_β), 7.31 (d, $J_{H,H}$ = 1.6 Hz, 1H; Ar-*H*), 7.30 (d, $J_{H,H}$ = 8.4 Hz, 1H; Ar-*H*), 7.19 (d, $J_{H,H}$ = 8.1 Hz, 1H; Ar-*H*), 7.09 (m, 2H; Ar-*H*), 6.70 (d, $J_{H,H}$ = 1.9 Hz, 1H; H_{pyrone}), 6.67 (d, $J_{H,H}$ = 16.0 Hz, 1H; H_α), 6.31 (d, $J_{H,H}$ = 1.8 Hz, 1H; H_{pyrone}), 5.32 (s, 2H; OCH_2O), 5.28 (s, 2H; OCH_2O), 3.98 (s, 3H; OCH_3), 3.97 (s, 3H; OCH_3), 3.54 (s, 3H; OCH_3), 3.53 (s, 3H; OCH_3). ^{13}C{^{1}H} NMR (100 MHz, $CDCl_3$): δ 180.3, 162.8, 161.8, 150.1, 150.0, 149.4, 148.3, 135.8, 129.4, 125.6, 121.7, 119.5, 118.3, 116.1, 116.0, 113.5, 110.5, 109.9, 109.3, 95.3, 95.2, 56.4, 56.1. ESI-MS (HR) *m/z*: $[M + H]^+$ calcd for $C_{25}H_{27}O_8$, 455.1700; found, 455.1696; *m/z*: $[M + Na]^+$ calcd for $C_{25}H_{26}NaO_8$, 477.1520; found, 477.1471; *m/z*: $[M + K]^+$ calcd for $C_{25}H_{26}KO_8$, 493.1259; found, 493.1220.

*4.2.12. (E)-2-(4-Hydroxy-3-methoxyphenyl)-6-(4-hydroxy-3-methoxystyryl)-4H-pyran-4-one, **1**.* To a stirred solution of (*E*)-2-(3-methoxy-4-(methoxymethoxy)phenyl)-6-(3-methoxy-4-(methoxymethoxy)styryl)-4*H*-pyran-4-one **22** (170 mg, 0.37 mmol) in MeOH (10 mL), an excess of HCl 1 M was added dropwise at room temperature (3 mL, 3.00 mmol, 8.02 equiv). The mixture was then refluxed with a heating mantle for 3 h, and the reaction advancement was followed by CCM (SiO_2 and EtOAc/MeOH, 95:5). At the end, the reaction was quenched with water (10 mL), and the precipitated product was filtered, washed with water, and finally dried to afford 2,6-γ-pyrone **1** as a yellow solid (125 mg, 91%). R_f: 0.33 (EtOAc/MeOH, 95:5). mp: 238 °C. IR (ATR, cm^{-1}): 3134 (br), 2932, 1641, 1628, 1595, 1508. ^{1}H NMR (400 MHz, DMSO-d_6): δ 9.87 (s, 1H; O*H*), 9.56 (s, 1H; O*H*), 7.58 (dd, $J_{H,H}$ = 8.3, 2.2 Hz, 1H; Ar-*H*), 7.52 (d, $J_{H,H}$ = 16.1 Hz, 1H; H_β), 7.52 (d, $J_{H,H}$ = 2.1 Hz, 1H; Ar-*H*), 7.37 (d, $J_{H,H}$ = 1.9 Hz, 1H; Ar-*H*), 7.19 (dd, $J_{H,H}$ = 8.3, 1.9 Hz, 1H; Ar-*H*), 7.01 (d, $J_{H,H}$ = 16.1 Hz, 1H; H_α), 6.99 (d, $J_{H,H}$ = 8.3 Hz, 1H; Ar-*H*), 6.86 (d, $J_{H,H}$ = 7.8 Hz, 1H; Ar-*H*), 6.85 (d, $J_{H,H}$ = 2.1 Hz, 1H; H_{pyrone}), 6.32 (d, $J_{H,H}$ = 2.2 Hz, 1H; H_{pyrone}), 3.94 (s, 3H; OCH_3), 3.89 (s, 3H; OCH_3). ^{13}C{^{1}H} NMR (100 MHz, DMSO-d_6): δ 180.0, 163.2, 162.6, 151.0, 149.6, 149.0, 148.95, 136.7, 127.7, 123.3, 122.9, 120.7, 117.9, 116.8, 116.6, 113.2, 111.8, 110.7, 109.8, 56.8, 56.7. ESI-MS (HR) *m/z*: $[M + H]^+$ calcd for $C_{21}H_{19}O_6$, 367.1176; found, 367.1184; *m/z*: $[M + Na]^+$ calcd for $C_{21}H_{18}NaO_6$, 389.0996; found, 389.0967.

*4.2.13. (Z)-2-(4-Hydroxy-3-methoxyphenyl)-6-(4-hydroxy-3-methoxystyryl)-4H-pyran-4-one, **1**.* An irradiation at 375 nm of the solution of **1** in DMSO led to **1**′ with a ratio: **1**/**1**′ 47:53. ^{1}H NMR (400 MHz, DMSO-d_6): δ 9.58 (s, 1H; O*H*), 9.36 (s, 1H; O*H*), 7.00 (d, $J_{H,H}$ = 1.5 Hz, 1H; Ar-*H*), 6.97 (d, $J_{H,H}$ = 1.9 Hz, 1H; Ar-*H*), 6.94 (d, $J_{H,H}$ = 12.0 Hz, 1H; H_β), 6.88 (m, 1H; Ar-*H*), 6.83 (d, $J_{H,H}$ = 2.2 Hz, 1H; H_{pyrone}), 6.80 (dd, $J_{H,H}$ = 8.4, 2.1 Hz, 1H; Ar-*H*), 6.77 (d, $J_{H,H}$ = 8.1 Hz, 1H; Ar-*H*), 6.70 (d, $J_{H,H}$ = 8.4 Hz, 1H; Ar-*H*), 6.33 (d, $J_{H,H}$ = 2.6 Hz, 1H; H_{pyrone}), 6.32 (d, $J_{H,H}$ = 12.0 Hz, 1H; H_α), 3.62 (s, 3H; OCH_3), 3.56 (s, 3H; OCH_3). ^{13}C{^{1}H} NMR (100 MHz, DMSO-d_6): δ 179.7, 163.3, 162.5, 150.8, 148.6, 148.4, 148.2, 138.7, 127.9, 123.5, 122.3, 120.5, 119.5, 116.3, 116.2, 115.7, 113.7, 110.1, 109.7, 56.3, 56.2. ESI-MS (HR) *m/z*: $[M + H]^+$ calcd for $C_{21}H_{19}O_6$, 367.1184; found, 367.1199; *m/z*: $[M + Na]^+$ calcd for $C_{21}H_{18}NaO_6$, 389.0996; found, 389.0967.

4.3. Computational Methodology. The GS minima of both isomers of the prepared γ-pyrone analogue of CC **1** was found under the framework of DFT, applying the B3LYP functional.[45]

To compute the absorption spectra of both isomers, time-dependent DFT (TD-DFT) was used. Different DFT functionals and basis sets were used to characterize the excitation of the molecule using Gaussian16 software.[46] As more remarkable, two main

https://doi.org/10.1021/acs.joc.1c00598
J. Org. Chem. 2021, 86, 8112−8126

behaviors can be shown. CAM-B3LYP strongly blue shifts the absorption maximum as is common for range-separate functionals.[47] It can be related to an improved representation of charge-transfer states compared to hybrid functionals that avoid the presence of significant intruder states, whose excitation energy would have been artificially lowered. In contrast, B3LYP better describes the shape of the absorption spectrum but yields in the presence of the intruder states due to an overstabilization of S_3 and an increase of the charge transfer states.[45]

To provide UV data more accurate to the one found experimentally, the vibrational and dynamical effects were considered around the Franck−Condon region *via* a Wigner distribution, using the NewtonX code to generate 100 structures.[48] The excited states were computed for each one through single-point calculations under vacuum at the CAM-B3LYP/6-31G* level of theory considering 20 roots, and finally convoluting all the Gaussian functions resulting from all transition energies and oscillator strengths.[49] Furthermore, this was carried out for the molecule in different solvents, using the optimized structure and the phase space for each solvent, not the vacuum frequencies. The solvent was included using the PCM[50] as implemented in Gaussian16,[46] using water, ethanol, dimethyl sulfoxide, and chloroform.

Fluorescence spectrum in vacuo was obtained from a Wigner distribution, sampling the vibrational space on the excited state minimum generating 100 structures. To compute the emission spectra, the first root which represents the S_0 to S_1 transition was only considered.

Coherently with an established protocol,[51−54] TPA cross sections have been simulated as a vertical transition from the ground-state equilibrium geometry only, that is, the Franck−Condon region, and was obtained at the TD-DFT level of theory through a quadratic response approach as implemented in the DALTON package.[55] The CAM-B3LYP exchange−correlation functional and the Pople 6-311++G(d,p) basis set were used, while excitation energies and cross sections have been calculated considering the effect of water solvent modeled at the PCM level.

4.4. Steady-State Measurements. *4.4.1. Absorption and Emission Spectra.* UV−visible spectra were recorded on a PerkinElmer Lambda 1050 UV−Vis−NIR spectrophotometer using a 1 cm optical path length cell at 25 °C, unless otherwise specified. The steady-state measurements were recorded on a Jobin Yvon Fluorolog-3 spectrofluorometer from Horiba Scientific and the FluorEssence program. The excitation source was a 450 W xenon lamp, and the detector used was R-928 operating at a voltage of 950 V. Excitation and emission slits width were 1 nm. The fluorescence quantum yields were determined using quinine sulphate as the standard (Φ = 0.53 in H_2SO_4, 0.05 M) using

$$\Phi_x = \Phi_s\left(\frac{\mathrm{Grad}_x}{\mathrm{Grad}_s}\right)\left(\frac{\eta_x^2}{\eta_s^2}\right)$$

where Φ, Grad, and η represent the fluorescence quantum yield, gradient from the plot of integrated fluorescence intensity versus absorbance, and refractive index of the solvent, respectively. The subscripts S and X denote the standard and test, respectively.

4.4.2. Kinetics and Fatigue Resistance. The photoisomerization was carried out on a 1.0 cm path length quartz cell placed on a four-sided cuvette holder (Cuvette Holder with Four Light Ports, CVH100 Thorlabs). Unless otherwise specified, the concentration of the samples was 40 μM. The kinetics of the photoisomerization process were measured by following the absorption spectrum during irradiation by selected LEDs, placed perpendicular to the absorbance measurement. To reach the PSS of the $E \rightarrow Z$ isomerization, the E-stereoisomer was illuminated within the $\pi-\pi^*$ band using an M375L4.1540 mW LED (LED Power Output 1540 mW, 2% power used) with a central wavelength of 375 nm and a bandwidth (FWHM) of 9 nm. For the reverse transformation, $Z \rightarrow E$ isomerization, the compound was excited within the n−π^* band using an M300L4.32 mW LED (LED Power Output: 47 mW, full power used) with a central wavelength of 300 nm and a bandwidth (FWHM) of 20 nm. In this case, the concentrations of compound **22** were 28.5 μM in DMSO, 33 μM in ethanol, 27 μM in acetonitrile, and 24 μM in chloroform. The thermal return process between *Z* and *E* isomers was analyzed by measuring the changes of the maximum absorbance wavelength at 25 and 40 °C, respectively. Kinetic monitoring of absorbance was performed using an Ocean Optics USB2000 + XR CCD sensor and kinetic constants were determined using "Biokine" software.

■ ASSOCIATED CONTENT

Supporting Information

The Supporting Information is available free of charge at https://pubs.acs.org/doi/10.1021/acs.joc.1c00598.

Benchmarking of DFT functionals, experimental procedures, ^{1}H and ^{13}C NMR spectra, physicochemical characterization of compound **1**, and Cartesian coordinates of compound **1** (PDF)

■ AUTHOR INFORMATION

Corresponding Authors

Andreea Pasc − *Université de Lorraine, CNRS, L2CM UMR 7053, F-54506 Vandœuvre-lès-Nancy, France;* orcid.org/0000-0002-9792-9144; Email: andreea.pasc@univ-lorraine.fr

Maxime Mourer − *Université de Lorraine, CNRS, L2CM UMR 7053, F-54506 Vandœuvre-lès-Nancy, France;* orcid.org/0000-0001-5272-4527; Email: maxime.mourer@univ-lorraine.fr

Authors

Jérémy Pecourneau − *Université de Lorraine, CNRS, L2CM UMR 7053, F-54506 Vandœuvre-lès-Nancy, France*

Raúl Losantos − *Université de Lorraine, CNRS, L2CM UMR 7053, F-54506 Vandœuvre-lès-Nancy, France; Université de Lorraine, CNRS, LPCT UMR 7019, F-54506 Vandœuvre-lès-Nancy, France*

Antonio Monari − *Université de Lorraine, CNRS, LPCT UMR 7019, F-54506 Vandœuvre-lès-Nancy, France;* orcid.org/0000-0001-9464-1463

Stéphane Parant − *Université de Lorraine, CNRS, L2CM UMR 7053, F-54506 Vandœuvre-lès-Nancy, France*

Complete contact information is available at: https://pubs.acs.org/10.1021/acs.joc.1c00598

Notes

The authors declare no competing financial interest.

■ ACKNOWLEDGMENTS

J.P. acknowledges French Ministry of Higher Education, Research and Innovation for his PhD grant. The authors greatly acknowledge the NMR Plateforme of Jean Barriol Institut and MassLor Spectrometry Plateforme of the University of Lorraine. The authors thank F. Dupire for performing mass spectrometry measurements. The authors gratefully acknowledge the University of Lorraine, CNRS, and the European Regional Development Funds (Programme opérationnel FEDER-FSE Lorraine et Massif des Vosges 2014-2020/"Fire Light" project: "Photo-bio-active molecules and nanoparticles") for financial support.

REFERENCES

(1) Gozem, S.; Schapiro, I.; Ferre, N.; Olivucci, M. The Molecular Mechanism of Thermal Noise in Rod Photoreceptors. *Science* **2012**, *337*, 1225−1228.

(2) Marazzi, M.; Gattuso, H.; Giussani, A.; Zhang, H.; Navarrete-Miguel, M.; Chipot, C.; Cai, W.; Roca-Sanjuán, D.; Dehez, F.; Monari, A. Induced Night Vision by Singlet-Oxygen-Mediated Activation of Rhodopsin. *J. Phys. Chem. Lett.* **2019**, *10*, 7133−7140.

(3) Sampedro, D.; Migani, A.; Pepi, A.; Busi, E.; Basosi, R.; Latterini, L.; Elisei, F.; Fusi, S.; Ponticelli, F.; Zanirato, V.; Olivucci, M. Design and Photochemical Characterization of a Biomimetic Light-Driven Z/E Switcher. *J. Am. Chem. Soc.* **2004**, *126*, 9349−9359.

(4) Bresolí-Obach, R.; Massad, W. A.; Abudulimu, A.; Lüer, L.; Flors, C.; Luis, J. G.; Rosquete, L. I.; Grillo, T. A.; Anamimoghadam, O.; Bucher, G.; Nonell, S. 9-Aryl-Phenalenones: Bioinspired Thermally Reversible Photochromic Compounds for Photoswitching Applications in the Pico-to Milliseconds Range. *Dyes Pigm.* **2021**, *186*, 109060.

(5) Romero, M. A.; Mateus, P.; Matos, B.; Acuña, Á.; García-Río, L.; Arteaga, J. F.; Pischel, U.; Basílio, N. Binding of Flavylium Ions to Sulfonatocalix[4]Arene and Implication in the Photorelease of Biologically Relevant Guests in Water. *J. Org. Chem.* **2019**, *84*, 10852−10859.

(6) Marazzi, M.; Francés-Monerris, A.; Mourer, M.; Pasc, A.; Monari, A. Trans-to-Cis Photoisomerization of Cyclocurcumin in Different Environments Rationalized by Computational Photochemistry. *Phys. Chem. Chem. Phys.* **2020**, *22*, 4749−4757.

(7) Adhikary, R.; Barnes, C. A.; Trampel, R. L.; Wallace, S. J.; Kee, T. W.; Petrich, J. W. Photoinduced Trans-to-Cis Isomerization of Cyclocurcumin. *J. Phys. Chem. B* **2011**, *115*, 10707−10714.

(8) Albota, M.; Beljonne, D.; Brédas, J. L.; Ehrlich, J. E.; Fu, J. Y.; Heikal, A. A.; Hess, S. E.; Kogej, T.; Levin, M. D.; Marder, S. R.; McCord-Maughon, D.; Perry, J. W.; Röckel, H.; Rumi, M.; Subramaniam, G.; Webb, W. W.; Wu, X. L.; Xu, C. Design of Organic Molecules with Large Two-Photon Absorption Cross Sections. *Science* **1998**, *281*, 1653−1656.

(9) Light, R. J.; Hauser, C. R. Aroylations of β-Diketones at the Terminal Methyl Group to Form 1,3,5-Triketones. Cyclizations to 4-Pyrones and 4-Pyridones. *J. Org. Chem.* **1960**, *25*, 538−546.

(10) Knight, J. D.; Metz, C. R.; Beam, C. F.; Pennington, W. T.; VanDerveer, D. G. New Strong Base Synthesis of Symmetrical 1,5-Diaryl-1,3,5-Pentanetriones from Acetone and Benzoate Esters. *Synth. Commun.* **2008**, *38*, 2465−2482.

(11) Solas, M.; Muñoz, M. A.; Suárez-Pantiga, S.; Sanz, R. Regiodivergent Hydration−Cyclization of Diynones under Gold Catalysis. *Org. Lett.* **2020**, *22*, 7681−7687.

(12) Xu, Y.-L.; Teng, Q.-H.; Tong, W.; Wang, H.-S.; Pan, Y.-M.; Ma, X.-L. Atom-Economic Synthesis of 4-Pyrones from Diynones and Water. *Molecules* **2017**, *22*, 109.

(13) Habert, L.; Cariou, K. Photoinduced Aerobic Iodoarene-Catalyzed Spirocyclization of N -Oxy-amides to N-Fused Spirolactams. *Angew. Chem.* **2021**, *133*, 173−177.

(14) Li, C.-S.; Lacasse, E. Synthesis of Pyran-4-Ones from Isoxazoles. *Tetrahedron Lett.* **2002**, *43*, 3565−3568.

(15) Thummala, Y.; Karunakar, G. V.; Doddi, V. R. DBU-Mediated Synthesis of Aryl Acetylenes or 1-Bromoethynylarenes from Aldehydes. *Adv. Synth. Catal.* **2019**, *361*, 611−616.

(16) Lautens, M.; Fang, Y.-Q.; Lifchits, O. Horner-Wadsworth-Emmons Modification for Ramirez Gem-Dibromoolefination of Aldehydes and Ketones Using P(Oi-Pr)3. *Synlett* **2008**, 413−417.

(17) Bryan, C. 2-(2,2-Dibromoethenyl)-benzenamine. *Org. Synth.* **2009**, *86*, 36−46.

(18) Tassano, E.; Alama, A.; Basso, A.; Dondo, G.; Galatini, A.; Riva, R.; Banfi, L. Conjugation of Hydroxytyrosol with Other Natural Phenolic Fragments: From Waste to Antioxidants and Antitumour Compounds: Conjugation of Hydroxytyrosol with Natural Phenolic Fragments. *Eur. J. Org. Chem.* **2015**, 6710−6726.

(19) Davyt, D.; Valdomir, G.; Padrón, J.; Padrón, J.; Martín, V. Oxazole/Thiazole and Triazole Hybrids Based on α-Amino Acids. *Synthesis* **2014**, *46*, 2451−2462.

(20) Morri, A. K.; Thummala, Y.; Doddi, V. R. The Dual Role of 1,8-Diazabicyclo[5.4.0]Undec-7-Ene (DBU) in the Synthesis of Terminal Aryl- and Styryl-Acetylenes via Umpolung Reactivity. *Org. Lett.* **2015**, *17*, 4640−4643.

(21) Miyakoshi, T.; Saito, S.; Kumanotani, J. A new synthesis of β-nitro carbonyl compounds from alkyl vinyl ketones with sodium nitrite-acetic acid in tetrahydrofuran. *Chem. Lett.* **1981**, *10*, 1677−1678.

(22) Rosini, G.; Ballini, R.; Sorrenti, P. A New Route to 1,4 -Diketones and Its Application to (z)-Jasmone and Dihydrojasmone Synthesis. *Tetrahedron* **1983**, *39*, 4127−4132.

(23) Mukaiyama, T.; Hoshino, T. The Reactions of Primary Nitroparaffins with Isocyanates. *J. Am. Chem. Soc.* **1960**, *82*, 5339−5342.

(24) Kulandai Raj, A. S.; Kale, B. S.; Mokar, B. D.; Liu, R.-S. Gold-Catalyzed N,O-Functionalizations of 6-Allenyl-1-Ynes with N -Hydroxyanilines To Construct Benzo[b]-Azepin-4-One Cores. *Org. Lett.* **2017**, *19*, 5340−5343.

(25) Pauli, L.; Tannert, R.; Scheil, R.; Pfaltz, A. Asymmetric Hydrogenation of Furans and Benzofurans with Iridium-Pyridine-Phosphinite Catalysts. *Chem.—Eur. J.* **2015**, *21*, 1482−1487.

(26) Rehbein, J.; Leick, S.; Hiersemann, M. Gosteli−Claisen Rearrangement: Substrate Synthesis, Simple Diastereoselectivity, and Kinetic Studies. *J. Org. Chem.* **2009**, *74*, 1531−1540.

(27) Persich, P.; Llaveria, J.; Lhermet, R.; de Haro, T.; Stade, R.; Kondoh, A.; Fürstner, A. Increasing the Structural Span of Alkyne Metathesis. *Chem.—Eur. J.* **2013**, *19*, 13047−13058.

(28) Zhao, H.-Y.; Wu, F.-S.; Yang, L.; Liang, Y.; Cao, X.-L.; Wang, H.-S.; Pan, Y.-M. Catalyst- and Solvent-Free Approach to 2-Arylated Quinolines via [5 + 1] Annulation of 2-Methylquinolines with Diynones. *RSC Adv.* **2018**, *8*, 4584−4587.

(29) Wang, T.; Shi, S.; Hansmann, M. M.; Rettenmeier, E.; Rudolph, M.; Hashmi, A. S. K. Synthesis of Highly Substituted 3-Formylfurans by a Gold(I)-Catalyzed Oxidation/1,2-Alkynyl Migration/Cyclization Cascade. *Angew. Chem., Int. Ed.* **2014**, *53*, 3715−3719.

(30) Hatano, M.; Sakamoto, T.; Mizuno, T.; Goto, Y.; Ishihara, K. Chiral Supramolecular U-Shaped Catalysts Induce the Multiselective Diels−Alder Reaction of Propargyl Aldehyde. *J. Am. Chem. Soc.* **2018**, *140*, 16253−16263.

(31) Zhang, S.; An, B.; Yan, J.; Huang, L.; Li, X. The Synthesis and Evaluation of New Benzophenone Derivatives as Tubulin Polymerization Inhibitors. *RSC Adv.* **2016**, *6*, 88453−88462.

(32) Pilkington, L. I.; Wagoner, J.; Kline, T.; Polyak, S. J.; Barker, D. 1,4-Benzodioxane Lignans: An Efficient, Asymmetric Synthesis of Flavonolignans and Study of Neolignan Cytotoxicity and Antiviral Profiles. *J. Nat. Prod.* **2018**, *81*, 2630−2637.

(33) Pang, Y.; An, B.; Lou, L.; Zhang, J.; Yan, J.; Huang, L.; Li, X.; Yin, S. Design, Synthesis, and Biological Evaluation of Novel Selenium-Containing Iso Combretastatins and Phenstatins as Antitumor Agents. *J. Med. Chem.* **2017**, *60*, 7300−7314.

(34) Sakata, Y.; Yasui, E.; Mizukami, M.; Nagumo, S. Cascade Reaction Including a Formal [5 + 2] Cycloaddition by Use of Alkyne-Co2(CO)6 Complex. *Tetrahedron Lett.* **2019**, *60*, 755−759.

(35) Rosiak, A.; Müller, R. M.; Christoffers, J. Synthesis of 2,3-Dihydrothiopyran-4-Ones from 3-Oxo-1-Pentene-4-Ynes. *Monatsh. Chem.* **2007**, *138*, 13−26.

(36) Tong, W.; Li, Q.-Y.; Xu, Y.-L.; Wang, H.-S.; Chen, Y.-Y.; Pan, Y.-M. An Unexpected Domino Reaction of β-Keto Sulfones with Acetylene Ketones Promoted by Base: Facile Synthesis of 3(2H)-Furanones and Sulfonylbenzenes. *Adv. Synth. Catal.* **2017**, *359*, 4025−4035.

(37) Ghandi, M.; Bayat, Y.; Teimuri-Mofrad, R. A novel method for the synthesis of formyl and hydroxymethyl derivatives of 4 h -pyran-4-one. *Org. Prep. Proced. Int.* **2002**, *34*, 525−530.

(38) Cao, Y.; Chen, L.; Xi, Y.; Li, Y.; Yan, X. Stimuli-Responsive 2,6-Diarylethene-4H-Pyran-4-One Derivatives: Aggregation Induced

https://doi.org/10.1021/acs.joc.1c00598
J. Org. Chem. 2021, 86, 8112−8126

Emission Enhancement, Mechanochromism and Solvatochromism. *Mater. Lett.* **2018**, *212*, 225−230.
(39) Xia, Y.; Wang, W. Asymmetric Synthesis of Machilin C and Its Analogue. *Chem. Pap.* **2010**, *64*, 630.
(40) Losantos, R.; Pecourneau, J.; Mourer, M.; Parant, S.; Pasc, A.; Monari, A. Trans-Cis Photoisomerization of Biomimetic Cyclocurcumin Analogous Rationalized by Molecular Modelling. *Phys. Chem. Chem. Phys.* **2021**, DOI: 10.1039/d1cp01224j.
(41) Pecourneau, J.; Losantos, R.; Monari, A.; Parant, S.; Pasc, A.; Mourer, M. Synthesis and Photoswitching Properties of Bioinspired Dissymmetric γ-Pyrone, Analogue of Cyclocurcumin. **2021**, chemrxiv.14236454.v1. ChemRxiv preprint.
(42) Faler, C. A.; Joullie, M. M. The Kulinkovich Reaction in the Synthesis of Constrained N,N-Dialkyl Neurotransmitter Analogues. *Org. Lett.* **2007**, *9*, 1987.
(43) Tangdenpaisal, K.; Sualek, S.; Ruchirawat, S.; Ploypradith, P. Factors Affecting Orthogonality in the Deprotection of 2,4-Di-Protected Aromatic Ethers Employing Solid-Supported Acids. *Tetrahedron* **2009**, *65*, 4316−4325.
(44) Schmittel, M.; Morbach, G.; Schenk, W. A.; Hagel, M. Synthesis, Thermal Reactivity and Structure of 1,2-Bis(4-Hydroxy-3-Methoxyphenylethynyl)Benzene. *J. Chem. Crystallogr.* **2005**, *35*, 373−379.
(45) Becke, A. D. Density-functional Thermochemistry. III. The Role of Exact Exchange. *J. Chem. Phys.* **1993**, *98*, 5648−5652.
(46) Frisch, M. J.; Trucks, G. W.; Schlegel, H. B. *Gaussian16*; Gaussian, Inc., 2016.
(47) Yanai, T.; Tew, D. P.; Handy, N. C. A New Hybrid Exchange−Correlation Functional Using the Coulomb-Attenuating Method (CAM-B3LYP). *Chem. Phys. Lett.* **2004**, *393*, 51−57.
(48) Barbatti, M.; Ruckenbauer, M.; Plasser, F.; Pittner, J.; Granucci, G.; Persico, M.; Lischka, H. A Surface-Hopping Program for Nonadiabatic Molecular Dynamics: Newton-X. *Wiley Interdiscip. Rev.: Comput. Mol. Sci.* **2014**, *4*, 26−33.
(49) Hehre, W. J.; Ditchfield, R.; Pople, J. A. Self—Consistent Molecular Orbital Methods. XII. Further Extensions of Gaussian—Type Basis Sets for Use in Molecular Orbital Studies of Organic Molecules. *J. Chem. Phys.* **1972**, *56*, 2257−2261.
(50) Tomasi, J.; Mennucci, B.; Cammi, R. Quantum Mechanical Continuum Solvation Models. *Chem. Rev.* **2005**, *105*, 2999−3094.
(51) Turan, H. T.; Eken, Y.; Marazzi, M.; Pastore, M.; Aviyente, V.; Monari, A. Assessing One- and Two-Photon Optical Properties of Boron Containing Arenes. *J. Phys. Chem. C* **2016**, *120*, 17916−17926.
(52) Marazzi, M.; Gattuso, H.; Monari, A.; Assfeld, X. Steady-State Linear and Non-Linear Optical Spectroscopy of Organic Chromophores and Bio-Macromolecules. *Front. Chem.* **2018**, *6*, 86.
(53) Gattuso, H.; Dumont, E.; Marazzi, M.; Monari, A. Two-Photon-Absorption DNA Sensitization via Solvated Electron Production: Unraveling Photochemical Pathways by Molecular Modeling and Simulation. *Phys. Chem. Chem. Phys.* **2016**, *18*, 18598−18606.
(54) Gattuso, H.; Monari, A.; Marazzi, M. Photophysics of Chlorin E6: From One- and Two-Photon Absorption to Fluorescence and Phosphorescence. *RSC Adv.* **2017**, *7*, 10992−10999.
(55) Aidas, K.; Angeli, C.; Bak, K. L.; Bakken, V.; Bast, R.; et al. The Dalton Quantum Chemistry Program System: The Dalton Program. *Wiley Interdiscip. Rev.: Comput. Mol. Sci.* **2014**, *4*, 269−284.

https://doi.org/10.1021/acs.joc.1c00598
J. Org. Chem. 2021, 86, 8112−8126